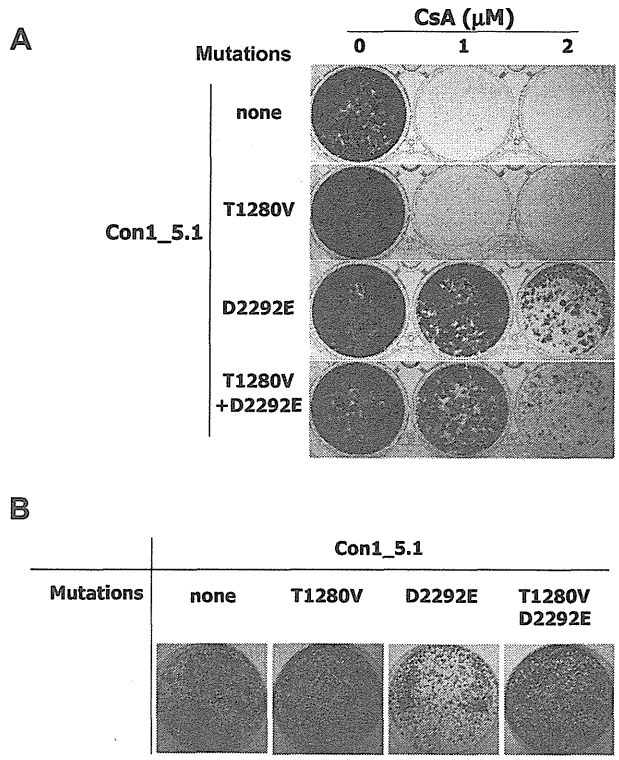

Fig. 3. (A) Resistance to CsA of T1280V and D2292E mutants. While under G418 selection, established replicon cells were treated with CsA at the indicated doses. (B) Standard methods described in Section 2 were used to determine the colony-forming abilities of T1280V and D2292E mutants.

known to confer CsA resistance to some HCV genotypes [25–28], and as a single mutation, it conferred CsA resistance to three separate HCV strains in our hands. In contrast, T1280V in NS3 was not previously identified as a CsA-resistance mutant, and in our hands, it had no impact on CsA resistance as a single mutation (Figs. 2E and 3A).

D2292E was the most significant resistance mutation in this study (Fig. 4C). This mutation is also significant in the regulation of HCV genome replication [29], and close to the CypA binding region [30] (Supplementary Fig. 1). With several genotypes (1a, 1b, 2a, 3, 4, and 6), D2292E is frequently observed after Debio-025 selection [28,31]. Other different mutations in NS5A and NS5B were identified in other studies of CsA resistance [7]; therefore, various mutations could influence HCV resistance to CsA.

In addition to the D2292E mutation, the T1280V mutation in NS3 was present in both clones #6 and #7. Despite its presence in both clones, it did not confer CsA resistance as a single mutant, nor did it enhance the effects of the NS5A CsA-resistant mutants (Fig. 2E). Instead, it partially rescued the colony-forming defect caused by D2292E (Fig. 3B). We used three assays—colony formation assay without CsA treatment (Fig. 3B), cell survival assay of established replicon cells with CsA and G418 dual-treatment (Fig. 3A), and HCV replication inhibition assay without G418 treatment (Fig. 2E and Table 2)—to evaluate the HCV replication competence of each of these two mutations (D2292E, T1280V). It is difficult to fully explain all of the results, and comparison of the two CsA-resistant clones (clone #6 and #7) leaves some questions unanswered. These clones were similar to each other when considering survival during CsA and G418 dual-treatment (Fig. 1B), but they show differences in their resistance in HCV sub-genome replication assay (Fig. 2B and E). Apparently, each mutation in clone #7, except for D2292E, had no effect on the results of the HCV sub-genome replication inhibition assay with CsA. These findings might suggest that these mutations were important to G418 resistance, but not to the resistance of HCV to CsA treatment. In contrast, each of three other mutations in NS5A (D2303H, S2362G, and E2414K) that were found in clone #6 were required for the maximum level of drug resistance conferred by a mutant NS5A in this study. To our knowledge, D2303H is a novel CsA-resistant mutation, and as a single mutation, it conferred CsA resistance comparable to D2292E. D2303H, like D2292E, was located in carboxy-terminal of domain II of NS5A, which is reportedly a CypA binding site [9]. S2362G and E2414K were mutations in domain III of NS5A, and these mutations may have influenced the peptidyl-prolyl isomerase enzymatic catalytic activity of CypA [22]. The V1681A mutation in NS4A identified in clone #6 greatly enhanced the CsA resistance of a HCV construct that had NS3 and NS5A replaced with Cs6#6 sequences (Fig. 2B–D). Though

Table 1
The list of each mutated amino acid sequences in 16 clones throughout whole non-structural region.

		NS3						4A	4B	NS5A											5B
A.A. No.		1062	1275	1280	1560	1609	1612	1681	1797	2109	2179	2197	2231	2269	2292	2303	2320	2362	2387	2414	2992
p5.1		V	D	T	S	K	I	V	I	D	S	P	L	S	D	D	K	S	S	E	M
Cs6#6	1	V	D	V	G	K	T	A	I	D	S	P	L	S	D	D	K	G	S	K	M
	2	V	D	V	S	E	I	V	I	N	S	P	L	S	D	D	K	S	S	E	M
	3	V	D	V	G	K	T	A	I	D	S	P	L	S	E	H	K	G	S	K	M
	4	V	D	V	G	K	T	A	I	D	S	P	L	S	E	H	K	G	S	K	M
	5	V	D	V	G	K	T	A	I	D	S	P	L	S	E	H	K	G	S	K	M
	6	V	D	V	G	K	T	A	I	E	S	P	L	S	E	H	K	G	S	K	M
	7	V	D	V	G	K	T	A	I	E	S	P	L	S	E	H	K	G	S	K	M
	8	V	D	V	G	K	T	A	I	D	S	P	L	S	E	H	K	G	S	K	M
Cs6#7	1	I	G	V	S	E	I	V	I	N	S	P	P	P	E	D	K	S	P	G	T
	2	V	D	V	S	E	I	V	I	N	S	P	P	P	E	D	K	S	P	G	T
	3	I	G	V	S	K	I	V	V	N	P	L	L	S	E	D	T	S	S	E	M
	4	I	G	V	S	K	I	V	V	D	P	L	L	S	E	D	M	S	S	E	M
	5	I	G	V	S	K	I	V	V	D	P	L	L	S	E	D	T	S	S	E	M
	6	I	G	V	S	K	I	V	V	D	P	L	L	S	E	D	T	S	S	E	T
	7	I	G	V	S	K	I	V	V	D	P	L	L	P	E	D	K	S	P	G	T
	8	V	D	V	S	E	I	V	I	N	S	P	P	P	E	D	K	S	P	G	T

The two gray-highlighted lines were selected as the representative sequences of CsA_6μM_#6 and #7 and used to generate the derivative constructs.

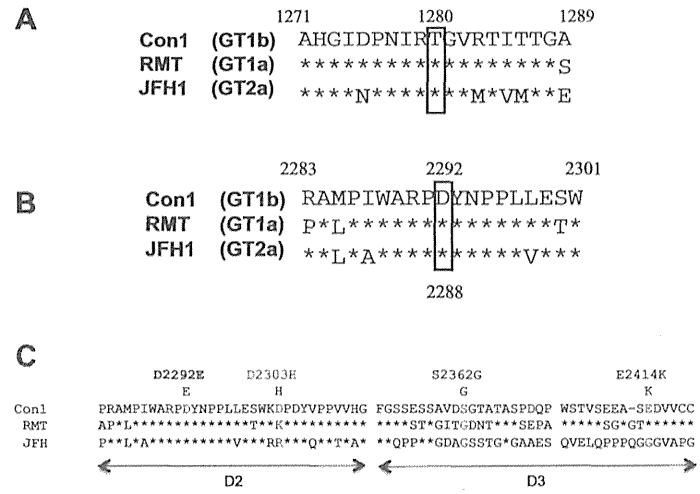

Fig. 4. Amino acid sequences of HCV-RMT-tri (GT1a) and HCV-JFH1 (GT2a) around (A) T1280V and (B) D2292E. (C) Location of the CsA resistant mutations in NS5A. Amino acid sequences around the positions of four CsA resistant mutations.

Table 2
Evaluation of resistance to CsA of mutants that have single mutations or combinations of multiple mutations.

	Mutations		IC_{50} (μm)	Fold change
	NS3	NS5A		
RMT-tri (RMT, GT1a)	–	–	0.79	1.0
	–	D2292E	2.1	2.7
	T1280I	–	0.96	1.2
	T1280I	D2292E	2.46	3.1
	T1280V	–	0.91	1.2
	T1280V	D2292E	2.54	3.2
JFH1 (JFH1, GT2a)	–	–	0.49	1.0
	–	D2292E	1.3	2.7
	T1280I	–	0.51	1.0
	T1280I	D2292E	1.38	2.8
	T1280V	–	0.69	1.4
	T1280V	D2292E	1.2	2.4

Threonine at site 1280 (RMT-tri or JFH1) were mutated to isoleucine (adaptive mutation of Con1 replicon) or valine (major mutation of CsA resistant clones). Aspartic acid at 2292 was mutated to glutamic acid.

Table 3
Evaluation of amino acid mutations in NS5A that conferred CysA resistance.

	Mutations in NS5A				IC_{50} (μm)	Fold change
	D2292E	D2303H	S2362G	E2414K		
Con1_5.1 (GT1b)					0.11	1.0
	○				0.88	7.9
		○			0.52	4.7
			○		0.12	1.0
				○	0.30	2.7
		○	○	○	1.0	9.4
	○	○			1.8	16.6
	○		○		0.95	8.5
	○			○	1.5	13.1
	○	○	○	○	2.80	25.7

we have not assessed V1681A as single mutant, analyzing its mechanism of CsA resistance and its cooperation with other mutations in NS3 and NS5A must be worthwhile because V1681A greatly enhanced the CsA resistance of some constructs.

In all, we evaluated three cyclophilin inhibitors—CsA, NIM811, and Debio-025. Among them, Debio-025 showed the strongest inhibition (IC_{50} values to any mutants) and was tolerated by CsA-resistant mutations (IC_{50} index change values, Fig. 2 and

Table 4
Evaluation of amino acid mutations in NS5A that conferred NIM811 resistance.

	Mutations in NS5A				IC_{50} (μm)	Fold change
	D2292E	D2303H	S2362G	E2414K		
Con1_5.1 (GT1b)					0.054	1.0
	○				0.324	6.0
		○			0.184	3.4
			○		0.056	1.0
				○	0.125	2.3
		○	○	○	0.455	8.4
	○	○			0.635	11.8
	○		○		0.403	7.5
	○			○	0.599	11.1
	○	○	○	○	0.923	17.1

Table 5
Evaluation of amino acid mutations in NS5A that conferred Debio-025 resistance.

	Mutations in NS5A				IC_{50} (μm)	Fold change
	D2292E	D2303H	S2362G	E2414K		
Con1_5.1 (GT1b)					0.024	1.0
	○				0.095	4.0
		○			0.074	3.1
			○		0.028	1.2
				○	0.024	1.8
		○	○	○	0.139	5.8
	○	○			0.198	8.3
	○		○		0.139	5.8
	○			○	0.185	7.8
	○	○	○	○	0.263	11.0

Table 3–5). It was interesting that the resistant mutants differed so greatly in their tolerance of these three inhibitors because all three inhibitors have the same mode of action. Garcia-Rivera et al. concluded that CsA resistance of HCV mutants were solely derived from dependence of the NS5A proteins on cyclophilins [28]. Our results might indicate that other factors are important to CsA resistance, in addition to residual cyclophilin activity.

Drugs that are intended to treat chronic HCV infection and that target important nonstructural HCV proteins—the serine protease NS3/4A, the large phosphoprotein NS5A, or the RNA-dependent RNA polymerase NS5B—have reached the clinical trial stage of drug development [32–34]. Two oral HCV protease inhibitors were approved by the FDA, and some of the drugs could achieve a sus-

tained virologic response (SVR) [35]. However, to develop treatments that eradicate individual chronic HCV infections, additional studies on the emergence of drug-resistant HCV mutants and on the molecular interactions at HCV replication complexes are necessary.

Our new findings provided insights into the way by which HCV acquires resistance to cyclophilin inhibitors, and these insights will facilitate the development of this type of anti-HCV drug for clinical use.

Acknowledgments

The authors thank Debiopharm Corporation for providing Debio-025 and Novartis Pharmaceuticals for providing NIM811. We also thank Dr. Masahiro Shuda for his technical support and advice, and Mr. Seima Itami for fruitful discussions. This study was supported in part by grants from the Ministry of Education, Culture, Sports, Science, and Technology of Japan; the Program for Promotion of Fundamental Studies in Health Sciences of the National Institute of Biomedical Innovation of Japan; and the Ministry of Health, Labour and Welfare of Japan.

Appendix A. Supplementary data

Supplementary data associated with this article can be found, in the online version, at http://dx.doi.org/10.1016/j.bbrc.2014.04.053.

References

[1] M. Arai, Y. Tokunaga, A. Takagi, Y. Tobita, Y. Hirata, Y. Ishida, C. Tateno, M. Kohara, Isolation and characterization of highly replicable hepatitis C virus genotype 1a strain HCV-RMT, PLoS ONE 8 (2013) e82527.
[2] I. Saito, T. Miyamura, A. Ohbayashi, H. Harada, T. Katayama, S. Kikuchi, Y. Watanabe, S. Koi, M. Onji, Y. Ohta, et al., Hepatitis C virus infection is associated with the development of hepatocellular carcinoma, Proc. Natl. Acad. Sci. USA 87 (1990) 6547–6549.
[3] L. Gravitz, Introduction: a smouldering public-health crisis, Nature 474 (2011) S2–S4.
[4] M. Kohara, T. Tanaka, K. Tsukiyama-Kohara, S. Tanaka, M. Mizokami, J.Y. Lau, N. Hattori, Hepatitis C virus genotypes 1 and 2 respond to interferon-alpha with different virologic kinetics, J. Infect. Dis. 172 (1995) 934–938.
[5] P. Simmonds, J. Bukh, C. Combet, G. Deleage, N. Enomoto, S. Feinstone, P. Halfon, G. Inchauspe, C. Kuiken, G. Maertens, M. Mizokami, D.G. Murphy, H. Okamoto, J.M. Pawlotsky, F. Penin, E. Sablon, I.T. Shin, L.J. Stuyver, H.J. Thiel, S. Viazov, A.J. Weiner, A. Widell, Consensus proposals for a unified system of nomenclature of hepatitis C virus genotypes, Hepatology 42 (2005) 962–973.
[6] L.I. Backus, P.S. Belperio, T.A. Shahoumian, R. Cheung, L.A. Mole, Comparative effectiveness of the hepatitis C virus protease inhibitors boceprevir and telaprevir in a large U.S. cohort, Aliment. Pharmacol. Ther. 39 (1) (2014) 93–103.
[7] F. Fernandes, D.S. Poole, S. Hoover, R. Middleton, A.C. Andrei, J. Gerstner, R. Striker, Sensitivity of hepatitis C virus to cyclosporine A depends on nonstructural proteins NS5A and NS5B, Hepatology 46 (2007) 1026–1033.
[8] F. Yang, J.M. Robotham, H.B. Nelson, A. Irsigler, R. Kenworthy, H. Tang, Cyclophilin A is an essential cofactor for hepatitis C virus infection and the principal mediator of cyclosporine resistance in vitro, J. Virol. 82 (2008) 5269–5278.
[9] T.L. Foster, P. Gallay, N.J. Stonehouse, M. Harris, Cyclophilin A interacts with domain II of hepatitis C virus NS5A and stimulates RNA binding in an isomerase-dependent manner, J. Virol. 85 (2011) 7460–7464.
[10] R. Flisiak, A. Horban, P. Gallay, M. Bobardt, S. Selvarajah, A. Wiercinska-Drapalo, E. Siwak, I. Cielniak, J. Higersberger, J. Kierkus, C. Aeschlimann, P. Grosgurin, V. Nicolas-Metral, J.M. Dumont, H. Porchet, R. Crabbe, P. Scalfaro, The cyclophilin inhibitor Debio-025 shows potent anti-hepatitis C effect in patients coinfected with hepatitis C and human immunodeficiency virus, Hepatology 47 (2008) 817–826.
[11] S. Hopkins, B. DiMassimo, P. Rusnak, D. Heuman, J. Lalezari, A. Sluder, B. Scorneaux, S. Mosier, P. Kowalczyk, Y. Ribeill, J. Baugh, P. Gallay, The cyclophilin inhibitor SCY-635 suppresses viral replication and induces endogenous interferons in patients with chronic HCV genotype 1 infection, J. Hepatol. 57 (2012) 47–54.
[12] E. Lawitz, E. Godofsky, R. Rouzier, T. Marbury, T. Nguyen, J. Ke, M. Huang, J. Praestgaard, D. Serra, T.G. Evans, Safety, pharmacokinetics, and antiviral activity of the cyclophilin inhibitor NIM811 alone or in combination with pegylated interferon in HCV-infected patients receiving 14 days of therapy, Antiviral Res. 89 (2011) 238–245.
[13] N. Kato, M. Hijikata, Y. Ootsuyama, M. Nakagawa, S. Ohkoshi, T. Sugimura, K. Shimotohno, Molecular cloning of the human hepatitis C virus genome from Japanese patients with non-A, non-B hepatitis, Proc. Natl. Acad. Sci. USA 87 (1990) 9524–9528.
[14] D. Moradpour, F. Penin, C.M. Rice, Replication of hepatitis C virus, Nat. Rev. Microbiol. 5 (2007) 453–463.
[15] R.A. Love, O. Brodsky, M.J. Hickey, P.A. Wells, C.N. Cronin, Crystal structure of a novel dimeric form of NS5A domain I protein from hepatitis C virus, J. Virol. 83 (2009) 4395–4403.
[16] T.L. Tellinghuisen, J. Marcotrigiano, C.M. Rice, Structure of the zinc-binding domain of an essential component of the hepatitis C virus replicase, Nature 435 (2005) 374–379.
[17] S. Feuerstein, Z. Solyom, A. Aladag, A. Favier, M. Schwarten, S. Hoffmann, D. Willbold, B. Brutscher, Transient structure and SH3 interaction sites in an intrinsically disordered fragment of the hepatitis C virus protein NS5A, J. Mol. Biol. 420 (2012) 310–323.
[18] X. Hanoulle, D. Verdegem, A. Badillo, J.M. Wieruszeski, F. Penin, G. Lippens, Domain 3 of non-structural protein 5A from hepatitis C virus is natively unfolded, Biochem. Biophys. Res. Commun. 381 (2009) 634–638.
[19] Y. Liang, H. Ye, C.B. Kang, H.S. Yoon, Domain 2 of nonstructural protein 5A (NS5A) of hepatitis C virus is natively unfolded, Biochemistry 46 (2007) 11550–11558.
[20] Y. Shirota, H. Luo, W. Qin, S. Kaneko, T. Yamashita, K. Kobayashi, S. Murakami, Hepatitis C virus (HCV) NS5A binds RNA-dependent RNA polymerase (RdRP) NS5B and modulates RNA-dependent RNA polymerase activity, J. Biol. Chem. 277 (2002) 11149–11155.
[21] X. Hanoulle, A. Badillo, J.M. Wieruszeski, D. Verdegem, I. Landrieu, R. Bartenschlager, F. Penin, G. Lippens, Hepatitis C virus NS5A protein is a substrate for the peptidyl-prolyl cis/trans isomerase activity of cyclophilins A and B, J. Biol. Chem. 284 (2009) 13589–13601.
[22] D. Verdegem, A. Badillo, J.M. Wieruszeski, I. Landrieu, A. Leroy, R. Bartenschlager, F. Penin, G. Lippens, X. Hanoulle, Domain 3 of NS5A protein from the hepatitis C virus has intrinsic alpha-helical propensity and is a substrate of cyclophilin A, J. Biol. Chem. 286 (2011) 20441–20454.
[23] F. Yasui, M. Sudoh, M. Arai, M. Kohara, Synthetic lipophilic antioxidant BO-653 suppresses HCV replication, J. Med. Virol. 85 (2013) 241–249.
[24] T. Takeuchi, A. Katsume, T. Tanaka, A. Abe, K. Inoue, K. Tsukiyama-Kohara, R. Kawaguchi, S. Tanaka, M. Kohara, Real-time detection system for quantification of hepatitis C virus genome, Gastroenterology 116 (1999) 636–642.
[25] K. Goto, K. Watashi, D. Inoue, M. Hijikata, K. Shimotohno, Identification of cellular and viral factors related to anti-hepatitis C virus activity of cyclophilin inhibitor, Cancer Sci. 100 (2009) 1943–1950.
[26] X. Puyang, D.L. Poulin, J.E. Mathy, L.J. Anderson, S. Ma, Z. Fang, S. Zhu, K. Lin, R. Fujimoto, T. Compton, B. Wiedmann, Mechanism of resistance of hepatitis C virus replicons to structurally distinct cyclophilin inhibitors, Antimicrob. Agents Chemother. 54 (2010) 1981–1987.
[27] L. Coelmont, X. Hanoulle, U. Chatterji, C. Berger, J. Snoeck, M. Bobardt, P. Lim, I. Vliegen, J. Paeshuyse, G. Vuagniaux, A.M. Vandamme, R. Bartenschlager, P. Gallay, G. Lippens, J. Neyts, DEB025 (Alisporivir) inhibits hepatitis C virus replication by preventing a cyclophilin A induced cis–trans isomerisation in domain II of NS5A, PLoS ONE 5 (2010) e13687.
[28] J.A. Garcia-Rivera, M. Bobardt, U. Chatterji, S. Hopkins, M.A. Gregory, B. Wilkinson, K. Lin, P.A. Gallay, Multiple mutations in hepatitis C virus NS5A domain II are required to confer a significant level of resistance to alisporivir, Antimicrob. Agents Chemother. 56 (2012) 5113–5121.
[29] D. Ross-Thriepland, Y. Amako, M. Harris, The C terminus of NS5A domain II is a key determinant of hepatitis C virus genome replication, but is not required for virion assembly and release, J. Gen. Virol. 94 (2013) 1009–1018.
[30] H. Grise, S. Frausto, T. Logan, H. Tang, A conserved tandem cyclophilin-binding site in hepatitis C virus nonstructural protein 5A regulates Alisporivir susceptibility, J. Virol. 86 (2012) 4811–4822.
[31] I.U. Ansari, R. Striker, Subtype specific differences in NS5A domain II reveals involvement of proline at position 310 in cyclosporine susceptibility of hepatitis C virus, Viruses 4 (2012) 3303–3315.
[32] D.R. Bobeck, R.F. Schinazi, S.J. Coats, Advances in nucleoside monophosphate prodrugs as anti-HCV agents, Antivir. Ther. 15 (2010) 935–950.
[33] R. De Francesco, G. Migliaccio, Challenges and successes in developing new therapies for hepatitis C, Nature 436 (2005) 953–960.
[34] Z. Huang, M.G. Murray, J.A. Secrist 3rd, Recent development of therapeutics for chronic HCV infection, Antiviral Res. 71 (2006) 351–362.
[35] M. Radkowski, J.F. Gallegos-Orozco, J. Jablonska, T.V. Colby, B. Walewska-Zielecka, J. Kubicka, J. Wilkinson, D. Adair, J. Rakela, T. Laskus, Persistence of hepatitis C virus in patients successfully treated for chronic hepatitis C, Hepatology 41 (2005) 106–114.

OPEN ACCESS Freely available online

PLOS | ONE

B-Cell-Intrinsic Hepatitis C Virus Expression Leads to B-Cell-Lymphomagenesis and Induction of NF-κB Signalling

Yuri Kasama[1], Takuo Mizukami[2], Hideki Kusunoki[2], Jan Peveling-Oberhag[3], Yasumasa Nishito[4], Makoto Ozawa[6,7], Michinori Kohara[5], Toshiaki Mizuochi[2], Kyoko Tsukiyama-Kohara[6,7]*

1 Department of Experimental Phylaxiology, Faculty of Life Sciences, Kumamoto University, Kumamoto-shi, Kumamoto, Japan, **2** Department of Research on Blood and Biological Products, National Institute of Infectious Diseases, Musashi-Murayama-shi, Tokyo, Japan, **3** Department of Internal Medicine, Goethe-University Hospital, Frankfurt, Germany, **4** Center for Microarray Analysis, Tokyo Metropolitan Institute of Medical Science, Kamikitazawa, Tokyo, Japan, **5** Department of Microbiology and Cell Biology, Tokyo Metropolitan Institute of Medical Science, Kamikitazawa, Tokyo, Japan, **6** Transboundary Animal Diseases Center, Joint Faculty of Veterinary Medicine, Kagoshima University, Kagoshima, Japan, **7** Laboratory of Animal Hygiene, Joint Faculty of Veterinary Medicine, Kagoshima University, Kagoshima, Japan

Abstract

Hepatitis C virus (HCV) infection leads to the development of hepatic diseases, as well as extrahepatic disorders such as B-cell non-Hodgkin's lymphoma (B-NHL). To reveal the molecular signalling pathways responsible for HCV-associated B-NHL development, we utilised transgenic (Tg) mice that express the full-length HCV genome specifically in B cells and develop non-Hodgkin type B-cell lymphomas (BCLs). The gene expression profiles in B cells from BCL-developing HCV-Tg mice, from BCL-non-developing HCV-Tg mice, and from BCL-non-developing HCV-negative mice were analysed by genome-wide microarray. In BCLs from HCV-Tg mice, the expression of various genes was modified, and for some genes, expression was influenced by the gender of the animals. Markedly modified genes such as Fos, C3, LTβR, A20, NF-κB and miR-26b in BCLs were further characterised using specific assays. We propose that activation of both canonical and alternative NF-κB signalling pathways and down-regulation of miR-26b contribute to the development of HCV-associated B-NHL.

Citation: Kasama Y, Mizukami T, Kusunoki H, Peveling-Oberhag J, Nishito Y, et al. (2014) B-Cell-Intrinsic Hepatitis C Virus Expression Leads to B-Cell-Lymphomagenesis and Induction of NF-κB Signalling. PLoS ONE 9(3): e91373. doi:10.1371/journal.pone.0091373

Editor: Ranjit Ray, Saint Louis University, United States of America

Received December 16, 2013; **Accepted** February 10, 2014; **Published** March 20, 2014

Funding: This work was supported by grants from the Ministry of Education, Culture, Sports, Science and Technology of Japan (23590547) and the Ministry of Health, Labour and Welfare of Japan (H21-011). The funders had no role in study design, data collection and analysis, decision to publish, or preparation of the manuscript.

Competing Interests: The authors have declared that no competing interests exist.

* E-mail: kkohara@vet.kagoshima-u.ac.jp

Introduction

Approximately 200 million people are currently infected with the hepatitis C virus (HCV) worldwide [1]. HCV has been the major etiological agent of post-transfusion hepatitis and has frequently caused liver cirrhosis and hepatocellular carcinoma in chronic hepatitis C (CHC) patients [2,3]. Hepatocytes are considered to be the primary and major site of HCV replication; however, extrahepatic manifestations are commonly seen in CHC patients. For example, mixed cryoglobulinemia (MC), a systemic immune complex-mediated disorder characterised by B cell proliferation with the risk of evolving into overt B-cell non-Hodgkin's lymphoma (B-NHL), is frequently recognised in CHC patients [4–6]. We have previously demonstrated the presence of both HCV RNA and viral proteins in peripheral B cells of CHC patients [7], although the mode of HCV infection and possible HCV replication in peripheral B cells remains a matter of debate. Furthermore, in the last two decades, an array of epidemiological evidence has accumulated involving the association between HCV infection and the occurrence of several hematologic malignancies, most notably B-NHL [8], [9]. The most compelling argument for a causal relationship between HCV and the occurrence of B-NHL is made by interventional studies demonstrating that a sustained virologic response to antiviral treatments, including the interferon α-induced regression of HCV-associated lymphomas and viral relapse after the initial virologic response, led to lymphoma recurrence [10]. However, the mechanisms underlying the cause-and-effect relationship are mostly unknown.

One of the potential host factors involved in HCV-associated B-NHL development is activator protein 1 (AP-1), which is primarily composed of c-Jun, c-Fos, and JunB, while JunD or Fra-1, Fra-2 and FosB are involved less frequently [11]. AP-1 is involved in B cell lymphomagenesis, is repressed by B cell lymphoma-6 [12] and is inhibited by the overexpression of T cell leukaemia/lymphoma 1, which resulted in the enhancement of nuclear factor kappa B (NF-κB) [13].

NF-κB is a ubiquitously expressed transcription factor that regulates a wide array of cellular processes, including the immune response, cell growth and differentiation [14,15]. The activation of NF-κB is regulated by two distinct pathways termed the 'canonical' and the 'alternative' NF-κB signalling pathways. Representative stimulators of the canonical and alternative pathways are tumour necrosis factor αTNFα) and lymphotoxin α and β (LTα and LTβ), respectively [16]. Previous studies have demonstrated that NF-κB is activated via both the canonical [17,18] and alternative [19] pathways in chronic HCV infection

[17,18] and HCV-related B-NHL [20]. However, the key NF-κB-activating pathway involved in HCV-associated B-NHL remains unknown.

TNFα-induced protein 3 (TNFAIP3), also known as A20, was first identified as a TNF-induced cytoplasmic protein with zinc finger motifs [21]. A20 has since been described as playing a pivotal role in the negative regulation of inflammation by terminating the canonical NF-κB signalling pathway [22–24]. Recently, A20 has gained attention as a novel tumour suppressor. For example, A20 was reported to be frequently inactivated or even deleted from mantle-cell lymphoma [25,26] and diffuse large B-cell lymphoma (DLBCL) [27]. These findings raise the possibility that inactivation of A20 is, at least partially, responsible for lymphomagenesis [28–30]. Other investigators have subsequently confirmed these findings [27,31]. Moreover, A20 also regulates antiviral signalling [32] as well as programmed cell death [33–35].

microRNAs (miRNAs) play a role in controlling various biological functions, including cell differentiation, growth regulation and transcriptional regulation [36]. In general, the dysfunctional expression of miRNAs is considered to be a common hallmark of cancers, including lymphomas [37]. HCV has been shown to influence miRNA expression *in vivo* and *in vitro* and utilises the liver-specific microRNA miR-122 for its replication [38]. The expression of miRNAs is also known to involve NF-κB activation. For example, miR-125a and miR-125b, both of which are often duplicated and/or overexpressed in DLBCL, were shown to activate NF-κB by targeting the A20 [39] and NF-κB-mediated dysregulation of miRNAs observed in lymphoma[40]. Moreover, global miRNA expression profiling analysis revealed miR-26b down-regulation in HCV-related splenic marginal zone lymphomas (SMZL) [41]. The same miRNA was found to be downregulated in peripheral blood mononuclear cells (PBMCs) from HCV-positive MC and NHL subjects [42].

We recently established transgenic mice that express the full-length HCV genome specifically in B cells (HCV-Tg mice) and observed the incidence of non-Hodgkin type B-cell lymphoma (BCL), primarily DLBCL, within 600 days after birth in approximately 25% of the HCV-Tg mice [43]. This experimental model is a useful tool for analysing the mechanisms underlying the development of HCV-associated manifestations such as B-NHL. To reveal the molecular signalling pathways responsible for HCV-associated B-NHL development, we performed a comprehensive molecular analysis of BCLs in HCV-Tg mice using a genome-wide microarray. We also characterised miR-26b expression in BCLs from HCV-Tg mice. Our results suggest that the activation of both canonical and alternative NF-κB pathways is involved in HCV-associated B-NHL development.

Materials and Methods

Ethics Statement

This study was carried out in strict accordance with both the Guidelines for Animal Experimentation of the Japanese Association for Laboratory Animal Science and the Guide for the Care and Use of Laboratory Animals of the National Institutes of Health. All experiment protocols were approved by the institutional review boards of the regional ethics committees of Kumamoto University (A22-136) and Kagoshima University (H24-008).

Animal experiments

The full-length HCV genome (Rz) under the conditional Cre/*lox*P expression system [44] with mice expressing the Cre enzyme under the transcriptional control of the B lineage–restricted gene *CD19* [45] was established as RzCD19Cre mice [43]. Wild-type (WT), Rz, CD19Cre, RzCD19Cre mice (129/sv, BALB/c and C57BL/6J mixed background) were maintained in conventional animal housing under specific pathogen-free conditions. CD19Cre and RzCD19Cre mice were bred to be heterozygous for the *Cre* allele.

Isolation of B cells and their RNAs

Mouse B cells were isolated using MACS^R beads (Milteny Biotec, Bergisch Gladbach, Germany) and anti-CD19 antibody (Beckton Dickinson, Franklin Lake, NJ). For FACS analysis, B and T cell populations were characterised using FITC-conjugated anti-B220 antibody (Milteny Biotec) and phycoerythrin (PE)-conjugated anti-CD3 antibody (Milteny Biotec) (Figure S1A). B cell purity was routinely over 95%. Total RNA was extracted from the B cells using the acid guanidine thiocyanate phenol chloroform method [44,46]. The RNA integrity number was measured with an Agilent 2100 Bioanalyzer (Agilent Technologies, Santa Clara, CA), and samples with values over 8.0 were subjected to microarray analysis (Figure S1B).

Microarray analysis

For microarray analysis, total RNAs were extracted, and RNA integrity was assessed using a Bioanalyzer (Agilent Technologies). cRNA targets were synthesised and hybridised with Whole Mouse Genome Microarray (G4846A; Agilent Technologies), in accordance with the manufacturer's instructions. More than 2-fold changes in gene expression were considered to be significant. Array data were analysed using MetaCore™ software (Thomson Reuters Co., New York, NY). The results of microarray analysis

Table 1. Mice subjected to microarray analysis.

Pairing	Mouse genotype	Mouse (No)	Age (d)	Sex	Remarks
1	RzCD19Cre	24–1	748	male	HCV(+)BCL*
		59–1	723	male	
		69–5	710	male	
	RzCD19Cre	248–1	860	male	HCV(+) B cell
		288–3	472	male	
		299–1	385	male	
2	RzCD19Cre	307–2	212	male	HCV(+) B cell
		307–3	212	male	
	Rz, 4EBP(+/−)+	307–1	220	male	HCV(−) B cell
		312–1	220	male	
3	RzCD19Cre	54–1	724	female	HCV(+)BCL
		62–2	723	female	
	RzCD19Cre	308–4	219	female	HCV(+) B cell
		308–6	219	female	
4	RzCD19Cre	308–4	219	female	HCV(+) B cell
		308–6	219	female	
	Rz	308–1	219	female	HCV(−) B cell
		308–3	219	female	

*BCL: B cell lymphoma; +4EBP(+/−): heterozygous knockout of 4E-BP1 gene [73].

doi:10.1371/journal.pone.0091373.t001

A Disease network

Pairing 1 (HCV+B vs HCV+BCL, male)

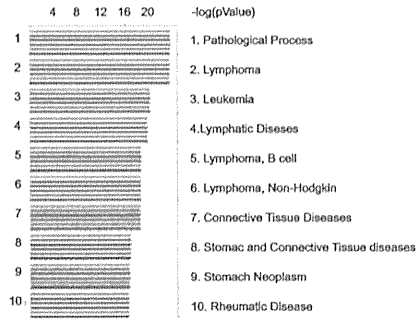

Pairing 2 (HCV+ vs HCV-, B cells, male)

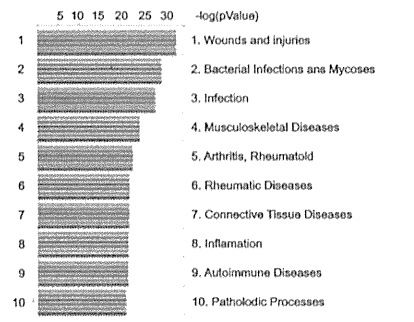

Pairing 3 (HCV+B vs HCV+BCL, female)

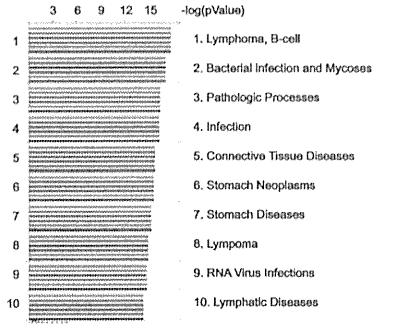

Pairing 4 (HCV+ vs HCV-, B cells, female)

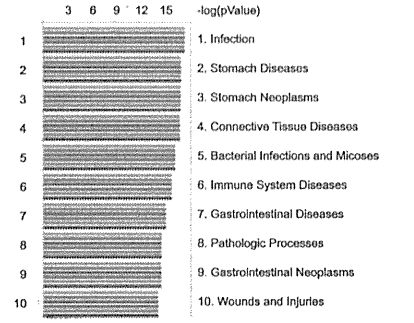

B Process network

Pairing 1 (HCV+B vs HCV+BCL, male)

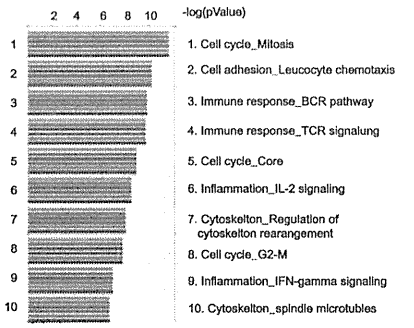

Pairing 2 (HCV+ vs HCV-, B cells, male)

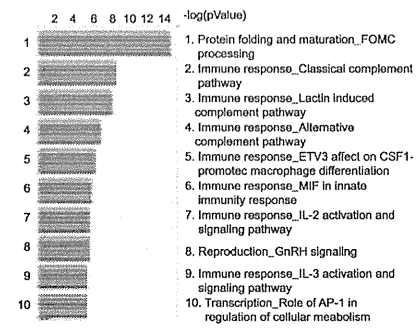

Pairing 3 (HCV+B vs HCV+BCL, female)

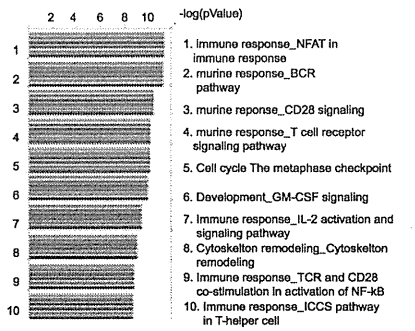

Pairing 4 (HCV+ vs HCV-, B cells, female)

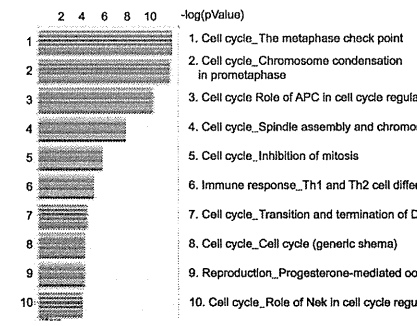

Figure 1. Data from array performed once with mixed RNA samples (Table 1) were analysed using MetaCore software. Signals were analysed in the disease network (**A**) and in the process network (**B**) the values for the microarray data [(Feature number; yellow), (Process Signal (635); blue), (Process signal (532); red), Test/Control (532/635); green], (Process Signal (635); orange), (Process signal (532); purple)] are indicated by coloured bars. Abbreviations: BCL = B cell lymphoma. Refer to Table 1 for construction of pairings.
doi:10.1371/journal.pone.0091373.g001

were registered in the Gene Expression Omnibus (GEO) database under the accession number GSE54722.

Quantitative RT-PCR

cDNA was synthesised from 0.5 or 1 μg of total RNA with a Superscript II kit (Life Technologies, Carlsbad, CA). TaqMan gene expression assays were custom-designed and manufactured by Life Technologies. RNA expression was quantified using the ABI 7500 real-time PCR system (Life Technologies) or the CFX96 system (BioRad, Hercules, CA).

Western blot analysis

Whole-cell proteins were extracted using RIPA buffer. Protein concentrations were determined using the BCA Protein assay Kit-Reducing Agent Compatible (Pierce Biotechnology, Rockford, IL). Samples (~10 μg) were loaded onto 10% SDS acrylamide gels, and gels were then transferred to PVDF membranes (Merck Millipore, Darmstadt, Germany). Membranes were blocked using 5% (w/v) non-fat milk for approximately 1 hour at room temperature and were then sequentially probed with primary and secondary antibodies at 4°C overnight and at room temperature for approximately 1 hour, respectively.

As primary antibodies, anti-A20 antibody (sc-166692; Santa Cruz Biotech, Dallas, TX), anti-A20 antibody (SAB3500036; Sigma-Aldrich, St. Louis, MO), anti-C3 antibody (D-19; Santa Cruz Biotech), anti-Fos (sc-52; Santa Cruz Biotech), anti-c-Jun(N) (sc-45; Santa Cruz Biotech) and anti-GAPDH-HRP (sc-20357; Santa Cruz Biotech) antibodies were used. Secondary antibodies used were horseradish peroxidase-coupled donkey anti-rabbit Ig (NA934; GE Healthcare, Buckinghamshire, UK) and horseradish peroxidase-coupled sheep anti-mouse Ig (NA931; GE Healthcare). Protein bands were detected and quantified using either Super-Signal West Dura or Femto Extended Duration Substrate (Pierce Biotechnology) with a LAS-3000 Image Analyzer (Fuji Film, Tokyo, Japan). Stripping and re-probing of the Western blots were performed using Re-blot plus mild antibody stripping solution (Merck Millipore).

Histological preparation

Liver, spleen, thymus and lymph nodes were harvested from HCV-Tg mice and fixed in 4% (wt/vol) paraformaldehyde in phosphate-buffered saline (pH 7.5) at 4°C for 24 hours. After fixation, samples were dehydrated in a graded ethanol series, cleared in xylene and embedded in paraffin, and 4-μm semi-thin sections were prepared using a carbon steel blade (Feather Safety Razor Co., Osaka, Japan) on a microtome (Yamato Kouki, Tokyo, Japan). Tissue sections were mounted on super-frosted glass slides coated with methyl-amino-silane (Matsunami Glass, Osaka, Japan). Histological images were acquired using an Olympus BX53 microscope (Olympus, Tokyo, Japan) equipped with 10×/0.30, 20×/0.50, 40×/0.75, and 100×/1.30 NA objective lenses. Images were captured using an Olympus DP73 (Olympus) under an Olympus FV1000 confocal microscope (Olympus).

Immunofluorescence

Anti-mouse NF-κB p65 antibody (Ab7970; Abcam, Cambridge, UK) and anti-mouse B220 (14-0452-81; eBioscience, San Diego, CA) were used as primary antibodies, and donkey anti-rat IgG-Alexa Fluor 488 [712-545-153; Jackson ImmunoResearch Laboratories Inc. (JIR), West Grove, PA], donkey anti-rabbit IgG-Alexa Fluor 488 (711-545-152; JIR), donkey anti-rat IgG-Cy3 (712-165-153; JIR) and donkey anti-rabbit IgG-Cy3 (711-165-152; JIR) were used as secondary antibodies. Staining was conducted as described previously [47]. Briefly, antigen retrieval was performed in a steam pressure cooker with prewarmed antigen retrieval buffer, citrate pH 6 (S203130; Dako, Glostrup, Denmark) at 95°C for 15 min. After blocking with 3% bovine serum albumin in phosphate-buffered saline, sections (4 μm) were incubated with anti-NF-κB, -Iκ-B, -B200 or -A20 antibodies at a 1:200 dilution each at 4°C overnight. Sections were incubated with secondary antibodies and anti-rat Alexa Fluor 488, -rabbit Alexa Fluor 488, -rat Alexa Fluor 546, and -rabbit Alexa Fluor 546 at room temperature for 2 hours. Nuclei were stained with Hoechst 333421 (H3570; Life Technologies).

Single assay stem-loop Q-RT-PCR/ miR-26b analysis

Formalin-fixed, paraffin-embedded (FFPE) splenic tissue from 24 animals (BCL HCV+, n = 8; BCL HCV-, n = 5; non-tumorous spleen HCV+/−, n = 11) was selected for miR-26b expression analysis. Total RNA was extracted using an RNeasy FFPE Kit (Qiagen, Hilden, Germany) in accordance with the manufacturer's protocol. Single assay stem-loop Q-RT-PCR (TaqMan MicroRNA assays, Life Technologies) was used to quantify miRNAs in accordance with the manufacturer's protocol. Total RNA input for each reaction was 50 ng. Expression was analysed for hsa-miR-26b and an endogenous control (snoRNA202). Each sample was analysed in triplicate, and delta C_t values were calculated using endogenous controls.

Statistics

For statistical analysis of NF-κB localisation, approximately 30–100 cells were randomly selected from each section area (two sections were used), and the cells double-positive for NF-κB and B220 were counted. All statistical analyses were performed using Prism software, version 5 (GraphPad, San Diego, CA). All experiments were independently performed three times, and a two-tailed Student *t*-test was applied to verify whether the results were significantly changed compared to the control ($P<0.05$).

Results

Characterisation of gene expression in B cells from HCV-Tg mice by microarray analysis

We previously established HCV-Tg mice that develop spontaneous BCL with a high penetrance (approximately 25%) [43]. To clarify the mechanisms of the HCV-associated B-NHL development using this mouse model, we performed a comprehensive gene expression analysis using a genome-wide microarray. B cells were isolated from BCL-developing HCV-Tg mice (Table 1, upper columns of pairing 1 and 3), from BCL-non-developing HCV-Tg mice (lower columns of pairing 1 and 3 and upper columns of pairing 2 and 4), and from BCL-non-developing HCV-negative mice (lower columns of pairing 2 and 4). RNA was purified from these B cells (Figure S1) and was characterised by microarray analysis (data not shown). In B cells isolated from BCL-non-developing HCV-Tg male mice, 455 and 863 genes were up-

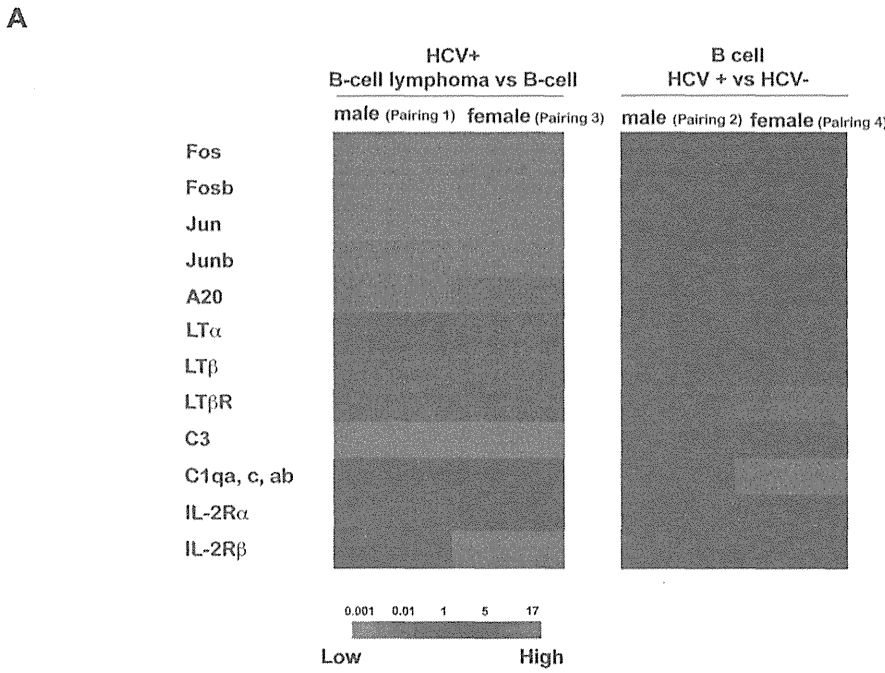
A
HCV+
B-cell lymphoma vs B-cell
B cell
HCV + vs HCV-
male (Pairing 1) female (Pairing 3)
male (Pairing 2) female (Pairing 4)
Fos
Fosb
Jun
Junb
A20
LTα
LTβ
LTβR
C3
C1qa, c, ab
IL-2Rα
IL-2Rβ
0.001 0.01 1 5 17
Low
High

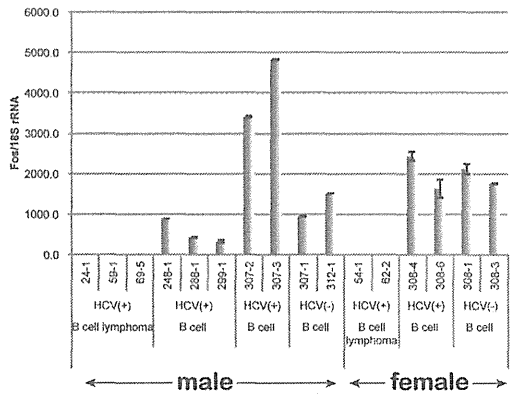
B
Fos/16S rRNA
6000.0
5000.0
4000.0
3000.0
2000.0
1000.0
0.0
24-1 59-1 69-5 248-1 288-1 299-1 307-2 307-3 307-1 312-1 54-1 62-2 308-4 308-6 308-1 308-3
HCV(+) HCV(+) HCV(+) HCV(-) HCV(+) HCV(+) HCV(+) HCV(-)
B cell lymphoma B cell B cell B cell B cell lymphoma B cell B cell
male
female

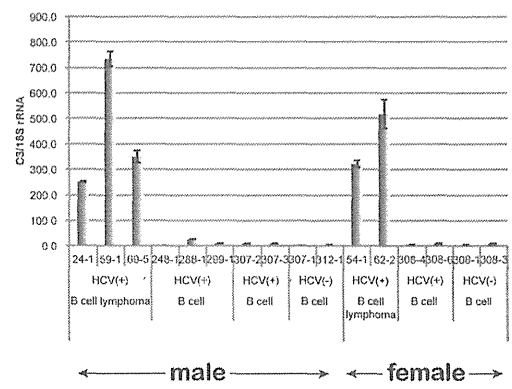
C
C3/16S rRNA
900.0
800.0
700.0
600.0
500.0
400.0
300.0
200.0
100.0
0.0
24-1 59-1 69-5 248-1 288-1 299-1 307-2 307-3 307-1 312-1 54-1 62-2 308-4 308-6 308-1 308-3
HCV(+) HCV(+) HCV(+) HCV(-) HCV(+) HCV(+) HCV(-)
B cell lymphoma B cell B cell B cell B cell lymphoma B cell B cell
male
female

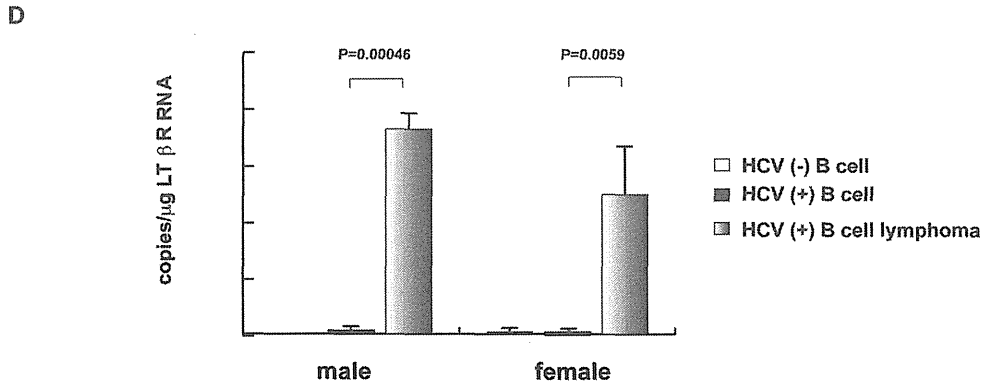
D
P=0.00046
P=0.0059
copies/μg LT β R RNA
male
female
HCV (-) B cell
HCV (+) B cell
HCV (+) B cell lymphoma

Figure 2. The expression of genes involved in oncogenic pathways associated with BCL. A: Highly modified gene signals in B cell lymphoma in RzCD19Cre mice BCL vs. B cells in RzCD19Cre male (Pair 1) or female (Pair 3) mice (left), and the genes modified by HCV expression in B cells in male (Pair 2) or female (Pair 4) (right). Red indicates the relative enhancement of the expression ratio of the processed signal (Test/Control, 532/635), and green indicates the relative reduction of expression. **B**: Quantification of Fos mRNA in HCV-, HCV+ B cells and HCV-Tg BCL in mice (numbers of individual mice were indicated) by quantitative RT-PCR. Fos mRNA was normalised against 18S rRNA, and the relative ratio was calculated. Vertical bars indicate S.D. **C**: Quantification of C3 mRNA in HCV-, HCV+ B cells and HCV-Tg BCL in mice. C3 mRNA was normalised against 18S rRNA, and relative ratio was calculated. Vertical bars indicate S.D. **D**: Quantification of LT βR mRNA in HCV-, HCV+ B cells and HCV-Tg BCL in mice by quantitative RT-PCR. RNA copies per total RNA (μg) were indicated and vertical bars indicate S.D.
doi:10.1371/journal.pone.0091373.g002

and down-regulated, respectively, compared with the HCV-negative counterparts (Table 1, pairing 2); whereas 133 and 331 genes were up- and down-regulated, respectively, in BCL-non-developing HCV-Tg female mice (Table 1, pairing 4). Furthermore, 1,682 and 2,383 genes were up- and down-regulated, respectively, in BCL-developing HCV-Tg male mice compared to their BCL-non-developing counterparts (Table 1, pairing 1); whereas 2,089 and 2,565 genes were up- and down-regulated, respectively, in BCL-developing HCV-Tg female mice (Table 1, pairing 3).

Metacore analysis of microarray results

In order to characterize the cellular processes affected by the gene expression changes, we carried out a pathway analysis of microarray data of pairings 1–4 (Table 1) using MetaCore™ software. This data mining revealed that lymphoma, leukaemia, B cell lymphoma, and lymphatic disease pathways were appreciably modified in pairings 1 and 3 with high frequency (Figure 1a). In pairings 2 and 4, the modifications involving wound healing and infection pathways were highlighted, respectively. In the process network, the cell cycle and immune response (B cell receptor, T cell receptor, and IL-2) pathways were greatly modified in pairings 1 and 3 (Figure 1b). The immune response (complement, macrophage, IL-2, and IL-3 in group 2; Th1 and Th2 in pairing), protein folding (in pairing 2), and cell cycle (in pairing 4) pathways were also modified.

Dysregulated genes in HCV-associated B-cell lymphoma

In addition to the pathways analysis, we also carefully examined the expression of genes involved in oncogenic pathways associated with BCL. Expression of Fos, Fosb, Jun and Junb was markedly down-regulated in BCL obtained from HCV-Tg mice (Figure 2a). Similarly, the expression of A20 and LTβ was greatly down-regulated in BCL (Figure 2a). In contrast, the expression of the LTβ receptor (LTβR), the IL-2 receptor α(IL-2Rα, IL-2Rβ and complement C3 was up-regulated in the examined BCLs (Figure 2a). While alterations in the gene expression of LTα and IL-2Rβ differed between males and females, the overall mRNA expression profile in the BCL analysed from HCV-Tg mice essentially showed no differences between male and female mice. In addition, clinically, there was no clear gender priority in HCV-NHL [48–50]. These results suggest that the molecular signalling pathways leading to HCV-associated B-NHL development are common to males and females.

In non-tumorous B cells from BCL-non-developing HCV-Tg male mice, the expression of LTβR and C3 was up-regulated when compared with HCV-negative counterparts (Figure 2a). In contrast, in female counterparts, the expression of LTβR and complements C1qa, c, and ab was down-regulated (Figure 2a, Pair. 4). These results suggest that the impact of HCV infection in B cells may be different between males and females.

Expression of Fos, C3, and LTβR genes in HCV-associated BCL

In order to validate the microarray results, levels of Fos and C3 mRNAs were quantified by real-time PCR. Striking down-regulation of Fos gene expression was observed in BCLs from HCV-Tg mice (Figure 2b). In contrast, C3 mRNA expression was markedly up-regulated in BCLs from HCV-Tg mice (Figure 2c). These results were consistent with the microarray data (Figure 2a, GEO accession number GSE54722). Similarly, the mRNA expression of the LTβR gene was significantly increased in HCV-associated BCLs (Figure 2d), confirming the microarray analysis results (Figure 2a). Importantly, these changes occurred in both male and female mice.

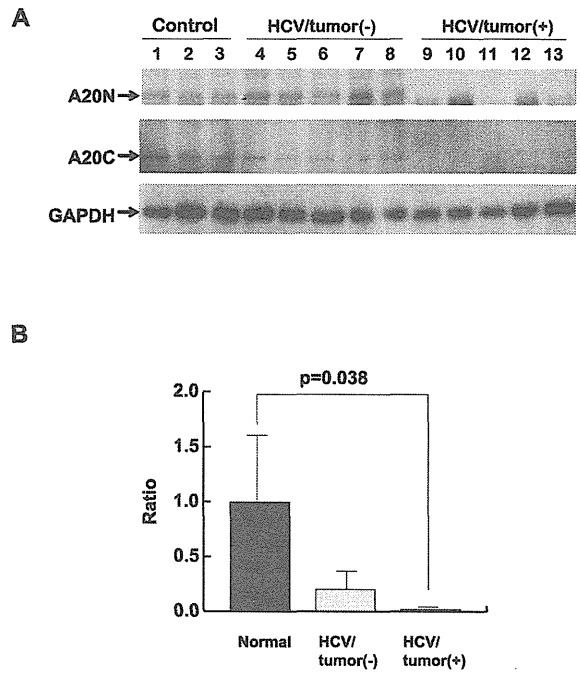

Figure 3. The expression of A20 in HCV-associated BCL. A: Expression levels of A20 in the spleen from RzCD19Cre mice with or without BCL. Whole-tissue extracts prepared from the spleen in CD19Cre mice (control, n = 3; lanes 1–3 217–2, 2 224–2, 224–3), RzCD19Cre mice without BCL (HCV/Tumour(-), n = 5; lanes 4–8 217–3, 224–4, 232–3, 254–4, 240–2) and RzCD19Cre mice with BCL (HCV/Tumour(+), n = 5; lanes 9–13 24–1, 56–5, 69–5, 59–1, 43–4) were subjected to SDS-PAGE and were analysed by immunoblotting using anti-N terminal (A20N), anti-C terminal A20 (A20C), and anti-GAPDH antibodies. GAPDH was used as protein loading control. **B**: Quantitation of A20 (N and C), the average is indicated and statistical analysis was performed. Vertical bars indicate S.D.
doi:10.1371/journal.pone.0091373.g003

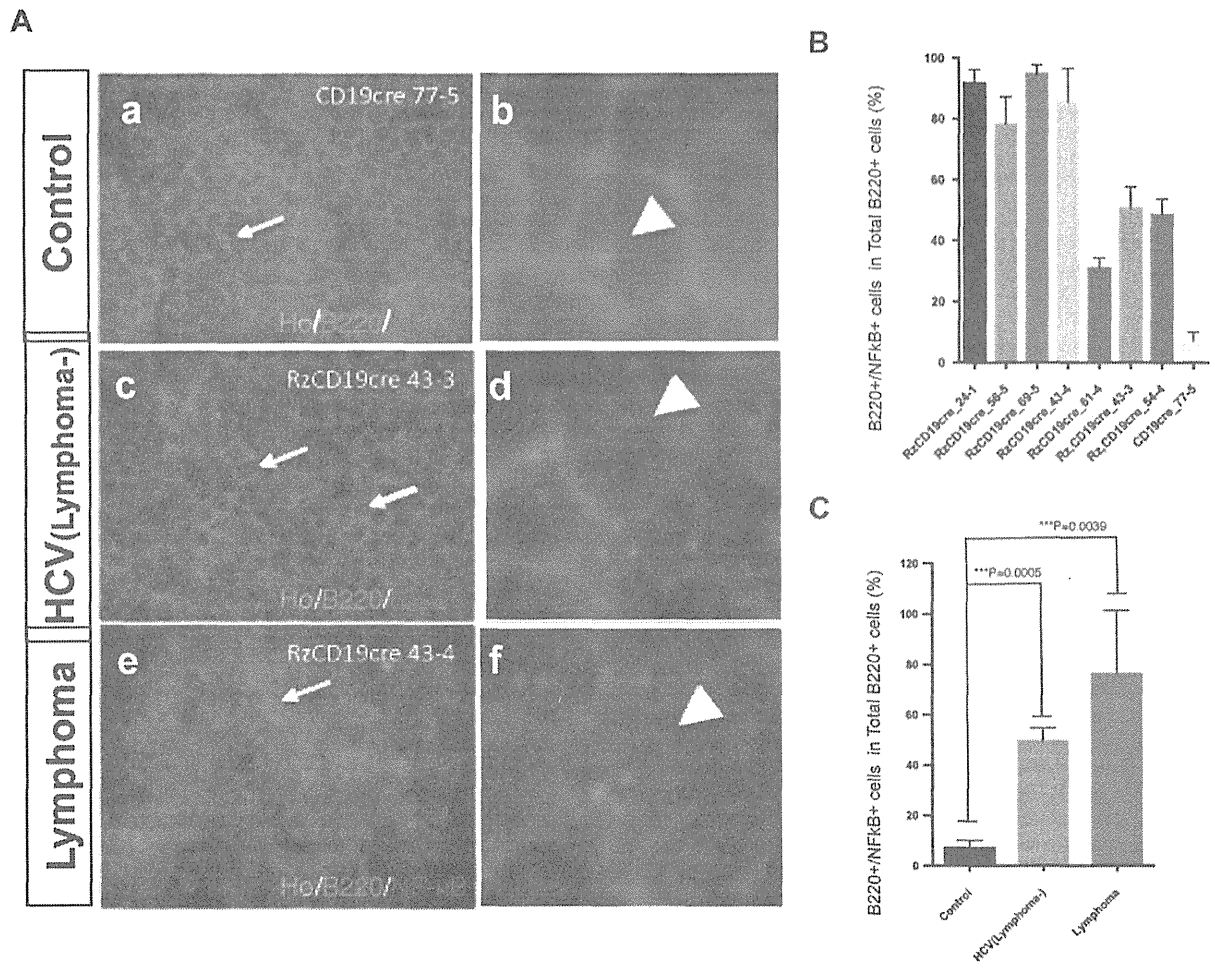

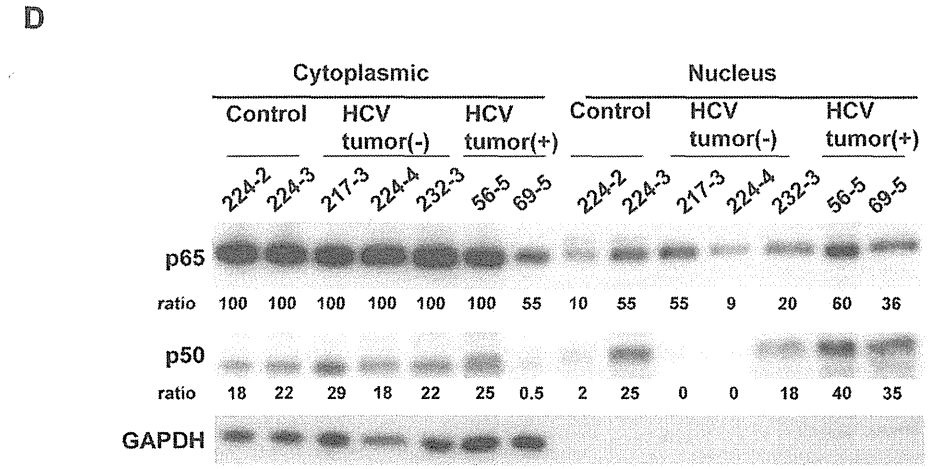

Figure 4. Double immunofluorescence localisation of B220 (Green) and NF-κB p65 (Red) in HCV-Tg mice and the fractionation analysis of mouse tissues. A: Co-localisation of NF-κB p65 immunoreactivity with B220 is indicated by arrows. (a–b) Cells double-positive for B220 and NF-κB in the control mouse (CD19cre). (c–d) Cells double-positive for B220 and NF-κB in the asymptomatic HCV-Tg mouse (RzCD19cre). (e–f) Cells double-positive for B220 and NF-κB in the lymphomatous HCV-Tg mouse (RzCD19cre). **B**: Quantitative analysis of the ratio of double-positive

cells among B220-positive cells in each HCV-Tg mouse. Bar graph indicates the percentage of cells with NF-κB p65 nuclear translocation in B220-positive cells. **C**: Bar graph shows the ratio of double-positive cells within the B220-positive cells in normal, asymptomatic and lymphomatous HCV-Tg mice. Ho: Hoechst33342 Data are presented as means ± S.E., * $P<0.05$, ** $P<0.01$, *** $P<0.001$. **D**: Western blot analysis: tissues from the spleen of controls (224–2, 3) or HCV-Tg mice without BCL (217–3, 224–4, 232–3) or with BCL (56–5, 69–5) were fractionated into nuclear and cytoplasmic fractions. NF-κB p50 and p65 were detected by antibodies. Relative ratios of quantitation by imager are indicated. GAPDH was detected as a loading control of the cytoplasmic fraction.
doi:10.1371/journal.pone.0091373.g004

Expression of A20 in HCV-associated BCL

In order to further validate the microarray results, we assessed A20 protein levels in BCLs isolated from HCV-Tg mice by Western blotting (Figure 3a). Two distinct anti-A20 antibodies recognising the N- (A20N) and C-terminal regions were used for the detection of A20. Regardless of the anti-A20 antibodies used, expression levels of A20 in BCL from HCV-Tg mice (Figure 3a, lanes 9 to 13) were markedly decreased when compared to splenocytes obtained from either BCL-non-developing HCV-negative mice (lanes 1 to 3) or from BCL-non-developing HCV-Tg mice (lanes 4 to 8). Quantitative analysis showed a significant decrease in A20 in BCLs obtained from HCV-Tg mice (Figure 3b). These results strongly suggest that the reduced expression of A20 is correlated with HCV-associated N-BHL development.

Nuclear localisation of NF-kB p65 in HCV-associated BCL

We next analysed the activation status of NF-κB by investigating the nuclear localisation of NF-κB p65 in cells positive for a B-cell marker molecule, B220, in BCLs isolated from HCV-Tg mice (Figure 4a). Quantitative analysis revealed that the ratio of cells double-positive for B220 and NF-κB p65 in the nuclei of the examined BCLs was significantly higher than the ratio in splenic tissue obtained from either BCL-non-developing HCV-negative mice or from BCL-non-developing HCV-Tg mice (Figures 4b and c). The fractionation assay showed that more NF-κB p50 and p65 were present in BCLs from HCV-Tg mice (Figure 4d). These results indicate the activation of NF-κB in HCV-associated BCL.

Expression of miR-26b in HCV-associated BCL

Recent studies have demonstrated that miR-26b is down-regulated in hepatocellular carcinoma [51], nasopharyngeal carcinoma [52], primary squamous cell lung carcinoma [53] and squamous cell carcinoma of the tongue [54]. In addition, miR-26b was down-regulated in HCV-positive SMZL when compared with HCV-negative counterparts [41] and in the PBMC of HCV-positive MC and NHL patients [42]. Therefore, we compared the expression levels of miR-26b in BCL from HCV-Tg mice with BCL from HCV-negative mice (i.e., spontaneously developed BCL) or in splenic tissue from BCL non-developing HCV-positive and -negative mice (Figure. 5). Interestingly, miR-26b expression was significantly down-regulated in BCLs from HCV-Tg mice. These results indicate that miR-26b is also down-regulated in HCV-associated BCL.

Discussion

In the present study, we identified differentially expressed genes in BCLs examined from HCV-Tg mice using a genome-wide microarray (Figures 1 and 2a, Table 1, and Figure S2). The microarray results for representative genes were validated at the RNA (Figures 2 and 5) and protein (Figures 3 and 4) levels. These findings helped dissect the molecular mechanisms underlying HCV-associated B-NHL development.

In the BCLs from HCV-Tg mice, the marked down-regulation of the Fos gene as well as other AP-1 protein genes (Fosb, Jun and Junb) was observed. Although AP-1 DNA binding activity was observed in Hodgkin-/multinuclear Reed-Stemberg cells and tissues from classical Hodgkin's disease, non-Hodgkin cell lines lacked the DNA binding activity of AP-1 [55]. Junb was weakly expressed in non-Hodgkin lymphomas of B-lymphoid origin; however, strong expression has been previously found in lymphomas that originated from the T-lymphoid lineage, and Junb selectively blocked B-lymphoid but not T-lymphoid cell proliferation ex vivo [56]. The BCL that developed in HCV-Tg mice was the non-Hodgkin type [43]; therefore, the decrease in AP-1 protein levels (Fos, Fosb, Jun, and Junb) may be crucial for lymphoma development.

In our previous study, soluble IL-2Rα levels were increased in BCL-developing HCV-Tg mice [43] Therefore, the up-regulation of IL-2Rα(Figure 2a) is potentially linked to the increase of soluble IL-2Rα, although further investigation is needed to clarify the details of this mechanism.

Expression of complement component C3 was significantly increased in BCLs isolated from HCV-Tg mice (Figure 2c). The presence of polymorphisms in complement system genes in non-Hodgkin lymphoma [57] suggests the involvement of complement in lymphoma development. The elevated C3 expression may be induced by TNF-α [58]. In addition, C3a, which is a cleavage product of C3, may contribute to the binding of NF-κB and AP-1 as shown previously [59].

The expression of LTβR, which is one of the key molecules in the alternative NF-κB signalling pathway [16], was significantly increased in BCLs from HCV-Tg mice (Figure 2d). HCV core proteins were reported to interact with the cytoplasmic domain of LTβR [60,61] and to enhance the alternative NF-κB signalling pathway [62]. The induction of LTβR by the HCV non-structural protein NS5B, and HCV RNA-dependent RNA polymerase, was also observed [63]. These findings suggest that the regulatory pathways involved in HCV infection also play a role in HCV-associated B-NHL development.

We observed several differences in the gene expression between male and female mice. Male HCV-negative mice showed up-regulation of LTβR and C3; however, female HCV-positive mice featured the downregulation of LTα and up-regulation of IL-2Rβ. Female HCV-Tg mice showed decreased overall survival in a previous study [43] and the above-mentioned gene dysregulations may contribute to this finding. However, the incidence of B-NHL between male and female mice did not show marked differences in the transgenic model [43]. Some clinical studies found gender-specific differences in the incidence of HCV-associated B-NHL and different effects of HCV on gene expression, which may also be dependent on gender [64]. However, meta-analyses did not provide consistent evidence for any gender preferences in HCV-NHL [48–50].

The down-regulation of A20, which is a ubiquitin-editing enzyme and tumour suppressor in various lymphomas [26], was observed in BCLs from HCV-Tg mice (Figures 3a and 3b). A20 has been reported to interact with the TNF receptor associated factor 2 (TRAF2), TRAF6, and the NF-κB essential modulator (NEMO). A20 inhibits NF-κB activation-induced by TNFα or by the overexpression of other proteins such as TRAF2 and receptor-interacting protein serine/threonine kinase 1 (RIPK1) proteins

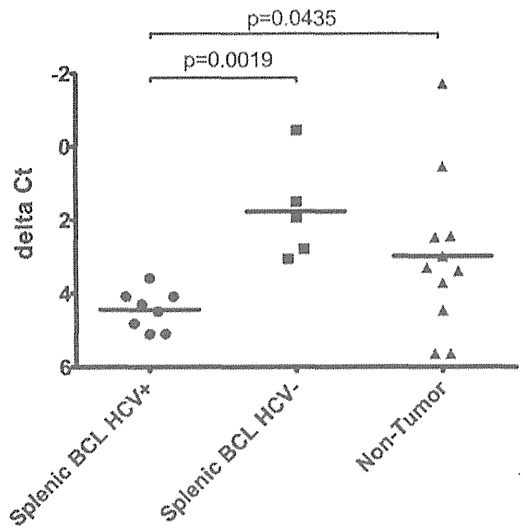

Figure 5. Quantification of miR-26b in BCL from HCV-positive and HCV-negative and non-tumour Tg mice. Formalin-fixed, paraffin-embedded (FFPE) splenic tissue from 24 animals (BCL HCV+, n = 8; BCL HCV-, n = 5; non-tumorous spleen HCV+/−, n = 11) was analysed for miR-26b expression by single assay stem-loop Q-RT-PCT by triplicate experiments. Data are shown as scatter dot-plots, and horizontal bar depicts the mean; y-axis: delta Ct (inverted scale) calculated in relation to endogenous control (snoRNA202). HCV-positive lymphoma tissue: filled circles; HCV-negative lymphoma tissue: filled squares; non-tumorous splenic tissue: filled triangles. P-values are shown in the graph.
doi:10.1371/journal.pone.0091373.g005

[65]. RIPK3 contributes to TNFR1-mediated RIPK1-dependent apoptosis and necroptosis [66]. RIPK2 (also known as RIP2) is also involved in B cell lymphoma cell survival and mediates the activation of NF-κB and MAPK pathways, associated with the TNF receptor family [67]. Therefore, suppression of A20 activates NF-κB by increasing nuclear translocation in tumour tissues.

Expression of miR-26b in BCLs obtained from HCV-Tg mice was significantly down-regulated (Figure 5). miR-26b is also down-regulated in numerous cancers, e.g., HCC [51], nasopharyngeal carcinomas [52], primary squamous cell lung carcinomas [53]and squamous cell carcinoma tongue [54]. In addition, c-Myc, which is up-regulated in various cancer types, has been shown to contribute to the reduction of miR-26a/b expression [68]. Notably, expression of miR-26b was significantly down-regulated in SMZL arising in HCV-positive patients [41]. Although the mechanisms of miR-26b-mediated tumourigenicity regulation are not fully understood, previous reports [69] and the present study have suggested a possible regulatory role of miR-26b in HCV-related lymphoma. Several candidates are reported to be targets of miR-26b. miR-26a and miR-26b are regulators of EZH2, which is the PRC2 polycomb repressive complex, is overexpressed in multiple cancers and is a target of the MYC oncogene [70]. In addition, lymphoid enhancer factor (LEF)-1 [42] and Nek6 [41] are targets of miR-26b. LEF-1 is a nuclear transcription factor that forms a complex with β-catenine and T-cell factor and induces transcription of cyclin D1 and c-myc. Nek6 is a kinase involved in the initiation of mitosis and is overexpressed in various tumours. The phosphatase and tensin homolog gene (PTEN) is also the putative target gene of miR-26b in adipogenic regulation [71] and cell growth [72].

This report is the first to demonstrate the possible involvement of networks of NF-κB, AP-1, complements and miR-26b in HCV-associated B-NHL (Figure S2). A future study focusing on the dysregulation of these networks and their modification by HCV may provide valuable information on improving therapy for HCV-associated B-NHL.

Supporting Information

Figure S1 **A**: B cells were isolated from mice using MACS beads and anti-CD19 antibody. The population of B cells was confirmed by staining with anti-B220 antibody. **B**: RNA integrity number (RIN) was measured using an Agilent 2100 Bioanalyzer (Agilent) for the estimation of purity.
(PDF)

Figure S2 **Possible pathways involved in BCL development. Both canonical and alternative NF-κB pathways may play a role.** Bold arrows indicate up-regulation or down-regulation. NIK; NF-κB-inducing kinase.
(PDF)

Acknowledgments

We would like to thank Drs. Kitabatake, Sato and Saito for their assistance with B cell separation and characterisation, and Professor Sakaguchi for his valuable encouragement.

Author Contributions

Conceived and designed the experiments: KT-K T. Mizuochi. Performed the experiments: YK T. Mizukami HK JP-O KT-K. Analyzed the data: YN JP-O T. Mizuochi KT-K. Contributed reagents/materials/analysis tools: MK. Wrote the paper: MO JP-O T. Mizuochi KT-K.

References

1. Shepard CW, Finelli L, Alter MJ (2005) Global epidemiology of hepatitis C virus infection. Lancet Infect Dis 5: 558–567.
2. Libra M, Gasparotto D, Gloghini A, Navolanic PM, De Re V, et al. (2005) Hepatitis C virus (HCV) I hepatitis C virus (HCV) infection and lymphoproliferative disorders. Front Biosci 10: 2460–2471.
3. Saito I, Miyamura T, Ohbayashi A, Harada H, Katayama T, et al. (1990) Hepatitis C virus infection is associated with the development of hepatocellular carcinoma. Proc Natl Acad Sci U S A 87: 6547–6549.
4. Silvestri F, Pipan C, Barillari G, Zaja F, Fanin R, et al. (1996) Prevalence of hepatitis C virus infection in patients with lymphoproliferative disorders. Blood 87: 4296–4301.
5. Ascoli V, Lo Coco F, Artini M, Levrero M, Martelli M, et al. (1998) Extranodal lymphomas associated with hepatitis C virus infection. Am J Clin Pathol 109: 600–609.
6. Mele A, Pulsoni A, Bianco E, Musto P, Szklo A, et al. (2003) Hepatitis C virus and B-cell non-Hodgkin lymphomas: an Italian multicenter case-control study. Blood 102: 996–999.
7. Ito M, Kusunoki H, Mizuochi T (2011) Peripheral B cells as reservoirs for persistent HCV infection. Front Microbiol 2: 177.
8. Dammacco F, Sansonno D, Piccoli C, Racanelli V, D'Amore FP, et al. (2000) The lymphoid system in hepatitis C virus infection: autoimmunity, mixed cryoglobulinemia, and Overt B-cell malignancy. Semin Liver Dis 20: 143–157.
9. Peveling-Oberhag J, Arcaini L, Hansmann ML, Zeuzem S (2013) Hepatitis C-associated B-cell non-Hodgkin lymphomas. Epidemiology, molecular signature and clinical management. J Hepatol 59: 169–177.
10. Hermine O, Lefrere F, Bronowicki JP, Mariette X, Jondeau K, et al. (2002) Regression of splenic lymphoma with villous lymphocytes after treatment of hepatitis C virus infection. N Engl J Med 347: 89–94.
11. Hess J, Angel P, Schorpp-Kistner M (2004) AP-1 subunits: quarrel and harmony among siblings. J Cell Sci 117: 5965–5973.
12. Vasanwala FH, Kusam S, Toney LM, Dent AL (2002) Repression of AP-1 function: a mechanism for the regulation of Blimp-1 expression and B lymphocyte differentiation by the B cell lymphoma-6 protooncogene. J Immunol 169: 1922–1929.

13. Pekarsky Y, Palamarchuk A, Maximov V, Efanov A, Nazaryan N, et al. (2008) Tcl1 functions as a transcriptional regulator and is directly involved in the pathogenesis of CLL. Proc Natl Acad Sci U S A 105: 19643–19648.
14. Ghosh S, Karin M (2002) Missing pieces in the NF-kappaB puzzle. Cell 109 Suppl: S81–96.
15. Sen R, Baltimore D (1986) Inducibility of kappa immunoglobulin enhancer-binding protein Nf-kappa B by a posttranslational mechanism. Cell 47: 921–928.
16. Bakkar N, Guttridge DC (2010) NF-kappaB signaling: a tale of two pathways in skeletal myogenesis. Physiol Rev 90: 495–511.
17. Sun B, Karin M (2008) NF-kappaB signaling, liver disease and hepatoprotective agents. Oncogene 27: 6228–6244.
18. Arsura M, Cavin LG (2005) Nuclear factor-kappaB and liver carcinogenesis. Cancer Lett 229: 157–169.
19. Haybaeck J, Zeller N, Wolf MJ, Weber A, Wagner U, et al. (2009) A lymphotoxin-driven pathway to hepatocellular carcinoma. Cancer Cell 16: 295–308.
20. De Re V, Caggiari L, Garziera M, De Zorzi M, Repetto O (2012) Molecular signature in HCV-positive lymphomas. Clin Dev Immunol 2012: 623465.
21. Opipari AW, Jr., Boguski MS, Dixit VM (1990) The A20 cDNA induced by tumor necrosis factor alpha encodes a novel type of zinc finger protein. J Biol Chem 265: 14705–14708.
22. Song HY, Rothe M, Goeddel DV (1996) The tumor necrosis factor-inducible zinc finger protein A20 interacts with TRAF1/TRAF2 and inhibits NF-kappaB activation. Proc Natl Acad Sci U S A 93: 6721–6725.
23. Lee EG, Boone DL, Chai S, Libby SL, Chien M, et al. (2000) Failure to regulate TNF-induced NF-kappaB and cell death responses in A20-deficient mice. Science 289: 2350–2354.
24. Heyninck K, Beyaert R (2005) A20 inhibits NF-kappaB activation by dual ubiquitin-editing functions. Trends Biochem Sci 30: 1–4.
25. Malynn BA, Ma A (2009) A20 takes on tumors: tumor suppression by an ubiquitin-editing enzyme. J Exp Med 206: 977–980.
26. Hymowitz SG, Wertz IE (2010) A20: from ubiquitin editing to tumour suppression. Nat Rev Cancer 10: 332–341.
27. Kato M, Sanada M, Kato I, Sato Y, Takita J, et al. (2009) Frequent inactivation of A20 in B-cell lymphomas. Nature 459: 712–716.
28. Honma K, Tsuzuki S, Nakagawa M, Karnan S, Aizawa Y, et al. (2008) TNFAIP3 is the target gene of chromosome band 6q23.3-q24.1 loss in ocular adnexal marginal zone B cell lymphoma. Genes Chromosomes Cancer 47: 1–7.
29. Honma K, Tsuzuki S, Nakagawa M, Tagawa H, Nakamura S, et al. (2009) TNFAIP3/A20 functions as a novel tumor suppressor gene in several subtypes of non-Hodgkin lymphomas. Blood 114: 2467–2475.
30. Schmitz R, Hansmann ML, Bohle V, Martin-Subero JI, Hartmann S, et al. (2009) TNFAIP3 (A20) is a tumor suppressor gene in Hodgkin lymphoma and primary mediastinal B cell lymphoma. J Exp Med 206: 981–989.
31. Compagno M, Lim WK, Grunn A, Nandula SV, Brahmachary M, et al. (2009) Mutations of multiple genes cause deregulation of NF-kappaB in diffuse large B-cell lymphoma. Nature 459: 717–721.
32. Parvatiyar K, Barber GN, Harhaj EW (2010) TAX1BP1 and A20 inhibit antiviral signaling by targeting TBK1-IKKi kinases. J Biol Chem 285: 14999–15009.
33. Parvatiyar K, Harhaj EW (2011) Regulation of inflammatory and antiviral signaling by A20. Microbes Infect 13: 209–215.
34. Tavares RM, Turer EE, Liu CL, Advincula R, Scapini P, et al. (2010) The ubiquitin modifying enzyme A20 restricts B cell survival and prevents autoimmunity. Immunity 33: 181–191.
35. Verstrepen L, Verhelst K, van Loo G, Carpentier I, Ley SC, et al. (2010) Expression, biological activities and mechanisms of action of A20 (TNFAIP3). Biochem Pharmacol 80: 2009–2020.
36. He L, Hannon GJ (2004) MicroRNAs: small RNAs with a big role in gene regulation. Nat Rev Genet 5: 522–531.
37. Lawrie CH (2007) MicroRNA expression in lymphoma. Expert Opin Biol Ther 7: 1363–1374.
38. Jopling CL, Yi M, Lancaster AM, Lemon SM, Sarnow P (2005) Modulation of hepatitis C virus RNA abundance by a liver-specific MicroRNA. Science 309: 1577–1581.
39. Kim SW, Ramasamy K, Bouamar H, Lin AP, Jiang D, et al. (2012) MicroRNAs miR-125a and miR-125b constitutively activate the NF-kappaB pathway by targeting the tumor necrosis factor alpha-induced protein 3 (TNFAIP3, A20). Proc Natl Acad Sci U S A 109: 7865–7870.
40. Hother C, Rasmussen PK, Joshi T, Reker D, Ralfkiaer U, et al. (2013) MicroRNA Profiling in Ocular Adnexal Lymphoma: A Role for MYC and NFKB1 Mediated Dysregulation of MicroRNA Expression in Aggressive Disease. Invest Ophthalmol Vis Sci 54: 5169–5175.
41. Peveling-Oberhag J, Crisman G, Schmidt A, Doring C, Lucioni M, et al. (2012) Dysregulation of global microRNA expression in splenic marginal zone lymphoma and influence of chronic hepatitis C virus infection. Leukemia 26: 1654–1662.
42. Fognani E, Giannini C, Piluso A, Gragnani L, Monti M, et al. (2013) Role of microRNA profile modifications in hepatitis C virus-related mixed cryoglobulinemia. PLoS One 8: e62965.
43. Kasama Y, Sekiguchi S, Saito M, Tanaka K, Satoh M, et al. (2010) Persistent expression of the full genome of hepatitis C virus in B cells induces spontaneous development of B-cell lymphomas in vivo. Blood 116: 4926–4933.
44. Tsukiyama-Kohara K, Tone S, Maruyama I, Inoue K, Katsume A, et al. (2004) Activation of the CKI-CDK-Rb-E2F pathway in full genome hepatitis C virus-expressing cells. J Biol Chem 279: 14531–14541.
45. Rickert RC, Roes J, Rajewsky K (1997) B lymphocyte-specific, Cre-mediated mutagenesis in mice. Nucleic Acids Res 25: 1317–1318.
46. Nishimura T, Kohara M, Izumi K, Kasama Y, Hirata Y, et al. (2009) Hepatitis C virus impairs p53 via persistent overexpression of 3beta-hydroxysterol Delta24-reductase. J Biol Chem 284: 36442–36452.
47. Yamazaki J, Mizukami T, Takizawa K, Kuramitsu M, Momose H, et al. (2009) Identification of cancer stem cells in a Tax-transgenic (Tax-Tg) mouse model of adult T-cell leukemia/lymphoma. Blood 114: 2709–2720.
48. Gisbert JP, Garcia-Buey L, Pajares JM, Moreno-Otero R (2003) Prevalence of hepatitis C virus infection in B-cell non-Hodgkin's lymphoma: systematic review and meta-analysis. Gastroenterology 125: 1723–1732.
49. Matsuo K, Kusano A, Sugumar A, Nakamura S, Tajima K, et al. (2004) Effect of hepatitis C virus infection on the risk of non-Hodgkin's lymphoma: a meta-analysis of epidemiological studies. Cancer Sci 95: 745–752.
50. de Sanjose S, Benavente Y, Vajdic CM, Engels EA, Morton LM, et al. (2008) Hepatitis C and non-Hodgkin lymphoma among 4784 cases and 6269 controls from the International Lymphoma Epidemiology Consortium. Clin Gastroenterol Hepatol 6: 451–458.
51. Ji J, Shi J, Budhu A, Yu Z, Forgues M, et al. (2009) MicroRNA expression, survival, and response to interferon in liver cancer. N Engl J Med 361: 1437–1447.
52. Ji Y, He Y, Liu L, Zhong X (2010) MiRNA-26b regulates the expression of cyclooxygenase-2 in desferrioxamine-treated CNE cells. FEBS Lett 584: 961–967.
53. Gao W, Shen H, Liu L, Xu J, Xu J, et al. (2011) MiR-21 overexpression in human primary squamous cell lung carcinoma is associated with poor patient prognosis. J Cancer Res Clin Oncol 137: 557–566.
54. Wong TS, Liu XB, Wong BY, Ng RW, Yuen AP, et al. (2008) Mature miR-184 as Potential Oncogenic microRNA of Squamous Cell Carcinoma of Tongue. Clin Cancer Res 14: 2588–2592.
55. Mathas S, Hinz M, Anagnostopoulos I, Krappmann D, Lietz A, et al. (2002) Aberrantly expressed c-Jun and JunB are a hallmark of Hodgkin lymphoma cells, stimulate proliferation and synergize with NF-kappa B. EMBO J 21: 4104–4113.
56. Szremska AP, Kenner L, Weisz E, Ott RG, Passegue E, et al. (2003) JunB inhibits proliferation and transformation in B-lymphoid cells. Blood 102: 4159–4165.
57. Bassig BA, Zheng T, Zhang Y, Berndt SI, Holford TR, et al. (2012) Polymorphisms in complement system genes and risk of non-Hodgkin lymphoma. Environ Mol Mutagen 53: 145–151.
58. Andoh A, Fujiyama Y, Hata K, Araki Y, Takaya H, et al. (1999) Counter-regulatory effect of sodium butyrate on tumour necrosis factor-alpha (TNF-alpha)-induced complement C3 and factor B biosynthesis in human intestinal epithelial cells. Clin Exp Immunol 118: 23–29.
59. Fischer WH, Jagels MA, Hugli TE (1999) Regulation of IL-6 synthesis in human peripheral blood mononuclear cells by C3a and C3a(desArg). J Immunol 162: 453–459.
60. Matsumoto M, Hsieh TY, Zhu N, VanArsdale T, Hwang SB, et al. (1997) Hepatitis C virus core protein interacts with the cytoplasmic tail of lymphotoxin-beta receptor. J Virol 71: 1301–1309.
61. Chen CM, You LR, Hwang LH, Lee YH (1997) Direct interaction of hepatitis C virus core protein with the cellular lymphotoxin-beta receptor modulates the signal pathway of the lymphotoxin-beta receptor. J Virol 71: 9417–9426.
62. You LR, Chen CM, Lee YH (1999) Hepatitis C virus core protein enhances NF-kappaB signal pathway triggering by lymphotoxin-beta receptor ligand and tumor necrosis factor alpha. J Virol 73: 1672–1681.
63. Simonin Y, Vegna S, Akkari L, Gregoire D, Antoine E, et al. (2013) Lymphotoxin Signaling Is Initiated by the Viral Polymerase in HCV-linked Tumorigenesis. PLoS Pathog 9: e1003234.
64. Vladareanu AM, Ciufu C, Neagu AM, Onisai M, Bumbea H, et al. (2010) The impact of hepatitis viruses on chronic lymphoproliferative disorders—preliminary results. J Med Life 3: 320–329.
65. Heyninck K, De Valck D, Vanden Berghe W, Van Criekinge W, Contreras R, et al. (1999) The zinc finger protein A20 inhibits TNF-induced NF-kappaB-dependent gene expression by interfering with an RIP- or TRAF2-mediated transactivation signal and directly binds to a novel NF-kappaB-inhibiting protein ABIN. J Cell Biol 145: 1471–1482.
66. Dondelinger Y, Aguileta MA, Goossens V, Dubuisson C, Grootjans S, et al. (2013) RIPK3 contributes to TNFR1-mediated RIPK1 kinase-dependent apoptosis in conditions of cIAP1/2 depletion or TAK1 kinase inhibition. Cell Death Differ 20: 1381–1392.
67. Cai X, Du J, Liu Y, Xia W, Liu J, et al. (2013) Identification and characterization of receptor-interacting protein 2 as a TNFR-associated factor 3 binding partner. Gene 517: 205–211.
68. Zhu Y, Lu Y, Zhang Q, Liu JJ, Li TJ, et al. (2012) MicroRNA-26a/b and their host genes cooperate to inhibit the G1/S transition by activating the pRb protein. Nucleic Acids Res 40: 4615–4625.
69. Ma YL, Zhang P, Wang F, Moyer MP, Yang JJ, et al. (2011) Human embryonic stem cells and metastatic colorectal cancer cells shared the common endogenous human microRNA-26b. J Cell Mol Med 15: 1941–1954.

70. Koh CM, Iwata T, Zheng Q, Bethel C, Yegnasubramanian S, et al. (2011) Myc enforces overexpression of EZH2 in early prostatic neoplasia via transcriptional and post-transcriptional mechanisms. Oncotarget 2: 669–683.
71. Song G, Xu G, Ji C, Shi C, Shen Y, et al. (2014) The role of microRNA-26b in human adipocyte differentiation and proliferation. Gene 533: 481–487.
72. Palumbo T, Faucz FR, Azevedo M, Xekouki P, Iliopoulos D, et al. (2013) Functional screen analysis reveals miR-26b and miR-128 as central regulators of pituitary somatomammotrophic tumor growth through activation of the PTEN-AKT pathway. Oncogene 32: 1651–1659.
73. Tsukiyama-Kohara K, Poulin F, Kohara M, DeMaria CT, Cheng A, et al. (2001) Adipose tissue reduction in mice lacking the translational inhibitor 4E-BP1. Nat Med 7: 1128–1132.

Research Article

Journal of Innate Immunity

J Innate Immun 2015;7:47–58
DOI: 10.1159/000365113

Received: March 14, 2014
Accepted after revision: June 9, 2014
Published online: August 8, 2014

A MAVS/TICAM-1-Independent Interferon-Inducing Pathway Contributes to Regulation of Hepatitis B Virus Replication in the Mouse Hydrodynamic Injection Model

Chean Ring Leong[a] Hiroyuki Oshiumi[a] Masaaki Okamoto[a] Masahiro Azuma[a]
Hiromi Takaki[a] Misako Matsumoto[a] Kazuaki Chayama[b] Tsukasa Seya[a]

[a]Department of Microbiology and Immunology, Graduate School of Medicine, Hokkaido University, Sapporo, and
[b]Department of Gastroenterology and Metabolism, Applied Life Sciences, Institute of Biomedical and Health Sciences, Hiroshima University, Hiroshima, Japan

Key Words
Type I interferon · Hepatitis B virus regulation · Toll/IL-1R homology domain-containing adaptor molecule 1 · Mitochondrial antiviral signaling protein · Pathogen-associated molecular patterns

Abstract
Toll-like receptors (TLRs) and cytoplasmic RNA sensors have been reported to be involved in the regulation of hepatitis B virus (HBV) replication, but remain controversial due to the lack of a natural infectious model. Our current study sets out to characterize aspects of the role of the innate immune system in eliminating HBV using hydrodynamic-based injection of HBV replicative plasmid and knockout mice deficient in specific pathways of the innate system. The evidence indicated that viral replication was not affected by MAVS or TICAM-1 knockout, but absence of interferon regulatory factor 3 (IRF-3) and IRF-7 transcription factors, as well as the interferon (IFN) receptor, had an adverse effect on the inhibition of HBV replication, demonstrating the dispensability of MAVS and TICAM-1 pathways in the early innate response against HBV. *Myd88*$^{-/-}$ mice did not have a significant increase in the initial viremia, but substantial viral antigen persisted in the mice sera, a response similar to *Rag2*$^{-/-}$ mice, suggesting that the MyD88-dependent pathway participated in evoking an adaptive immune response against the clearance of intrahepatic HBV. Taken together, we show that the RNA-sensing pathways do not participate in the regulation of HBV replication in a mouse model; meanwhile MyD88 is implicated in the HBV clearance.

Introduction

Hepatitis B virus (HBV) is a noncytopathic human DNA (hepadna) virus that infects hepatocytes causing acute and chronic hepatitis [1]. More than 360 million people are chronically infected with HBV worldwide. Although less than 5% of HBV-infected patients develop persistent infections that progress to liver cirrhosis and hepatocellular carcinoma, HBV causes about 20% of hepatocellular carcinoma deaths [2]. The adaptive immune response is widely acknowledged as pivotal in the defense against HBV. However, the role of innate immunity during HBV infection remains controversial since analysis in patients at the early stage of infection is unfeasible. In ad-

1662–811X/14/0071–0047$39.50/0

E-Mail karger@karger.com
www.karger.com/jin

Dr. Tsukasa Seya
Department of Microbiology and Immunology
Graduate School of Medicine, Hokkaido University
Kita-15, Nishi-7, Kita-ku, Sapporo 060-8638 (Japan)
E-Mail seya-tu@pop.med.hokudai.ac.jp

dition, no reliable cell-based in vitro infection system or convenient animal model is available.

During HBV infection, the HBV genome is delivered into the nucleus. Infection is defined by the formation of covalently closed circular DNA. Following formation of covalently closed circular DNA, viral mRNA and pregenomic RNA are transcribed [3, 4]. The pregenomic RNA is subsequently converted to a partially double-stranded genome by the viral DNA polymerase. Unlike other DNA viruses, HBV uses an RNA proviral intermediate that must be copied back into DNA for replication. Although these replication steps are sequestered in the nucleus of infected cells, cytoplasmic DNA/RNA sensors are reported to affect the efficacy of HBV replication [5, 6]. The association between cytoplasmic pattern recognition receptors and the dynamics of the HBV life cycle in HBV-infected cells needs to be clarified.

Viral RNA is sensed by the innate immune system by either Toll-like receptor 3 (TLR3) or cytoplasmic sensors such as retinoic acid-inducible gene-I (RIG-I) and melanoma differentiation-associated gene 5 (MDA5). RIG-I and MDA5 mainly participate in type I interferon (IFN) induction in conjunction with the adaptor molecule, mitochondrial antiviral signaling protein (MAVS; also called IPS-1, Cardif, or VISA) [7–9]. The Toll/IL-1R homology domain-containing adaptor molecule 1 (TICAM-1; also called TRIF) is the adaptor of TLR3, which senses viral RNA on the endosomal membrane [8–10]. Several DNA sensors, most of which signal through STING for type I IFN induction, have been reported in recent years [11]. A few reports have also mentioned that MAVS participates in DNA sensing in certain human cells whereby poly-dA/dT DNA is found to signal via RIG-I. Later, it was also shown that poly-dA/dT serves as a template for RNA polymerase III to make RIG-I ligands [12–14]. Nevertheless, this hypothesis is unresolved in mouse cells. Once stimulated by the viral DNA/RNA, these adaptor proteins activate IFN regulatory factor (IRF)-3 and IRF-7, which induce type I IFN production [7–9]. These pattern recognition receptor-mediated early innate immune responses are crucial in controlling viral replication and spread before the initiation of more specific and powerful adaptive immune responses [8, 9, 15].

Despite numerous studies on HBV pathogenesis, the putative molecular patterns of HBV that trigger cellular responses remain unknown. A few reports have suggested that the antiviral response against HBV is mediated by the RIG-I/MAVS pathway in the cytosol and its activation is blocked by HBV polymerase in infected cells [16–18]. However, no definitive evidence in vivo is available because analysis on the gene expression and effectors required for elimination of the replicative template has been especially difficult. Since viral clearance is a multifaceted process, we hydrodynamically injected a naked HBV plasmid DNA into wild-type (WT) and gene-disrupted mice deficient in TICAM-1, MAVS, TICAM-1/MAVS, IRF-3/IRF-7, IFNAR, MyD88, or RAG2 to identify and characterize the immunological events for HBV clearance. With the availability of various gene-disrupted mice, our study allows the identification of pathways crucial for the clearance of HBV.

Materials and Methods

Animal Studies

All mice were backcrossed with C57BL/6 mice more than seven times before use. *Ticam-1*$^{-/-}$ [19] and *Mavs*$^{-/-}$ [20] mice were generated in our laboratory as described previously, while *Ticam-1*$^{-/-}$ *Mavs*$^{-/-}$ mice were generated by crossing *Ticam-1*$^{-/-}$ mice with *Mavs*$^{-/-}$ mice. *Irf-3*$^{-/-}$/*Irf-7*$^{-/-}$ and *Ifnar*$^{-/-}$ mice were kindly provided by T. Taniguchi (University of Tokyo, Tokyo, Japan). *Myd88*$^{-/-}$ mice were provided by Drs. K. Takeda and S. Akira (Osaka University, Osaka, Japan). *Rag2*$^{-/-}$ mice were kindly provided by Dr. N. Ishii (Tohoku University, Sendai, Japan). Female C57BL/6J mice were purchased from CLEA Japan (Tokyo) and used at 7–9 weeks of age. All mice were maintained under specific pathogen-free conditions in the animal facility at Hokkaido University Graduate School of Medicine (Sapporo, Japan). Animal experiments were performed according to the guidelines set by the Animal Safety Center, Japan.

Hydrodynamic Transfection of Mice with HBV1.4 Plasmid

The pTER1.4xHBV plasmid containing 1.4-genome length sequences of HBV that were previously shown to produce a similar sedimentation in sucrose density gradient centrifugation to HBV extracted from the serum of carriers [21] was used in this study. A total of 50 μg of the plasmid was injected into the tail vein of 7- to 9-week-old mice in a volume of 2.0 ml of TransIT-QR hydrodynamic delivery solution (Mirus, USA). The total volume was delivered within 3–8 s. Plasmid DNA was prepared by using an Endo-Free plasmid system (Qiagen, Germany) according to the manufacturer's instructions.

Quantification of HBV DNA by Real-Time PCR

To determine the HBV DNA in the serum, 30 μl of each serum sample was pretreated with 20 units of DNase I (Roche, Germany) at 37°C overnight. The encapsidated viral DNA was extracted with the SMITEST kit (Genome Science Laboratories, Tokyo, Japan) following the manufacturer's instructions and dissolved in 20 μl of TE-buffer. The purified viral genome was quantified by real-time PCR using the SYBR green master mix (Life Technologies, USA) and the HBV-DNA-F/R primer (see suppl. table 1 for primer sequences; for all online suppl. material, see www.karger.com/doi/10.1159/000365113). Amplification conditions included initial denaturation at 95°C for 10 min, followed by 45 cycles of

denaturation at 95°C for 15 s, annealing at 58°C for 5 s, and extension at 72°C for 6 s. The lower detection limit of this assay is 1,000 copies.

Immunohistochemical Staining for HBV Core Antigen

For immunohistochemical staining of the HBV core antigen (HBcAg), mouse livers were fixed with 4% paraformaldehyde overnight, cryoprotected in 30% sucrose, and sectioned at a thickness of 10 μm using Leica cryostat and mounted on Superfrost glass slides. Sections were incubated with the primary antibody (anticore polyclonal rabbit antibody, DAKO) overnight, followed by incubation with an immunoperoxidase technique involving avidin-biotin peroxidase complexes (Vectastain ABC kit; Vector Laboratories, Burlingame, Calif., USA) according to a method reported previously [22].

HBV Surface Antigen Antigenemia

Mice were bled on the days mentioned after injection of pTER-1.4xHBV and serum was isolated by centrifugation. Concentration of HBV surface antigen (HBsAg) in the serum was quantified by sandwich ELISA in commercial ELISA kits following the manufacturer's protocol (XpressBio, USA). The reporting unit is the signal/cutoff ratio of the 1,000-fold diluted serum at an O.D. of 450 nm.

Southern Blotting to Detect Intracapsid HBV DNA

Viral DNA was isolated from intracellular viral capsids and detected with a specific DIG-labeled probe as described previously [21]. In brief, to isolate the viral DNA, mouse livers were homogenized and subjected to overnight sodium dodecyl sulfate-proteinase K digestion followed by phenol extraction and ethanol precipitation. Twenty micrograms of the isolated DNA was separated in 1% agarose gel, transferred onto Immobilon-Ny+ charged nylon membrane (Milipore), and detected with a full-length HBV-DNA probe labeled by the DIG DNA labeling and detection kit (Roche Diagnostics, Basel, Switzerland) according to the instructions provided by the manufacturer.

Anti-HBs Antibody ELISA

IgG antibodies specific for HBsAg were detected by ELISA as described previously [23] with slight modification. A 96-well plate was coated with antigen of HBs in carbonate buffer and followed by blocking of 2% BSA. Plasma samples were diluted 5× and then incubated in the antigen-coated wells for 3 h at room temperature. A horseradish peroxidase-conjugated goat anti-mouse IgGγ (Southern Biotechnology, USA) and TMB were used to develop the signal. Plates were read at 450 nm. Normal mouse plasma was used to generate cutoff values. The antibody titers are reported as the reciprocal of A_{450} (sample)/A_{450} (2.1' normal mouse average) at which samples with a value >1 were considered to have scored positive.

Quantitative HBV or Cytokines mRNA in the Organs

Each organ was extracted from the mice on the days mentioned after hydrodynamic injection of the HBV plasmid. Total RNA of the organs was isolated with TRIzol according to the manufacturer's protocol. Using 0.5–1 μg of total RNA as a template, cDNA was obtained using a high-capacity cDNA transcription kit (Applied Biosystems) according to manufacturer's instructions. qPCR was performed using a Step One real-time PCR system (Applied Biosystems). The expression of cytokine mRNA was normalized to that of β-actin mRNA in each organ, and the fold increase was determined by dividing the expression in each sample by that of the mice receiving the control plasmid. The primer sequences are described in online supplementary table 1.

Quantitative cGAS, STING, and MAVS Expression in Cell Lines

Total RNA was isolated from L929 cells, RAW264.7 cells, immortalized mouse hepatocytes, Huh7 cells, and HepG2 cells with TRIzol according to the manufacturer's protocol. Using 0.5–1 μg of total RNA as a template, cDNA was obtained using a high-capacity cDNA transcription kit (Applied Biosystems) according to manufacturer's instruction. qPCR was performed using a Step One real-time PCR system (Applied Biosystems). The expression of each targeted mRNA was normalized to that of β-actin mRNA in each sample and shown as a relative expression. The primer sequences are described in online supplementary table S1.

Reporter Gene Assay

To prepare the HBV RNA, immortalized mouse hepatocytes previously established in our laboratory [24] were transfected with either control plasmid or pTER1.4xHBV. Total RNA containing the HBV RNA was isolated after 12 h and confirmed with RT-PCR, while the RNA transfected with only control plasmid was used as a control. The isolated RNA was later used as stimuli for the reporter gene assay of IFN-β. Briefly, the immortalized hepatocytes were again transfected with the reporter plasmids. After 16 h, the immortalized hepatocytes were transfected with the stimuli including PIC, a control plasmid, HBV RNA, and pTER1.4xHBV using FuGENE HD (Roche). Cells were lysed at the time point mentioned using a passive lysis buffer, and Firefly and Renilla luciferase activities were determined using a dual-luciferase reporter assay kit. Firefly luciferase activity was normalized by Renilla luciferase activity and was expressed as the fold stimulation relative to activity in nonstimulated cells.

Statistical Analysis

The statistical significance of the obtained data in this study was analyzed using a two-tail unpaired t test and $p < 0.05$ was regarded as statistically significant.

Results

MAVS and TICAM-1 Are Dispensable in Suppressing HBV Replication

We hydrodynamically transfected replication-competent HBV DNA into *Mavs*$^{-/-}$ or *Ticam-1*$^{-/-}$ and *Mavs*$^{-/-}$/*Ticam-1*$^{-/-}$ mice to access the role of these viral RNA-sensing pathways in response to HBV. Serum HBsAg and HBV-DNA levels were monitored regularly as surrogate markers of HBV replication in vivo. WT mice displayed acute self-limiting hepatitis with peak HBs antigenemia on day 4 after DNA injection (fig. 1a–c). Subsequently, HBsAg in sera decreased and terminated by day 11. *Mavs*$^{-/-}$ and *Ticam-1*$^{-/-}$ mice displayed HBsAg clearance

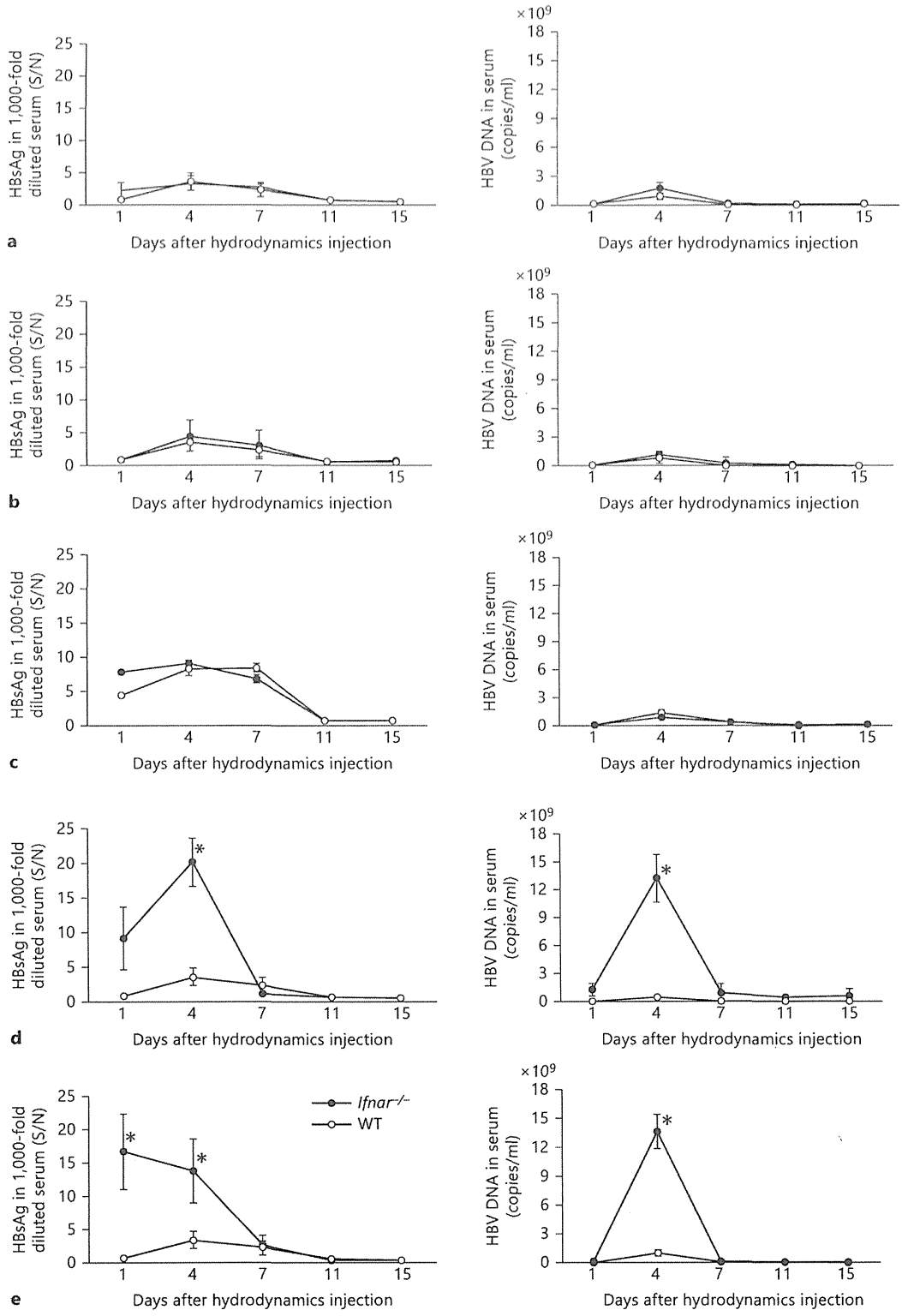

1

(*For legend see next page.*)

kinetics that closely paralleled the WT mice response (fig. 1a, b, left panels). Serum HBV-DNA levels were quantified using real-time PCR. The average titer of serum HBV DNA in 15 WT mice injected with HBV DNA was below 1×10^4 copies/ml 1 day after injection and reached 2×10^9 copies/ml 4 days after injection (fig. 1a–c, right panels). At later time points, most mice showed no detectable virus titer. Similar results were obtained with *Mavs*$^{-/-}$ and *Ticam-1*$^{-/-}$ mice (fig. 1a, b). The serum HBV-DNA and HBsAg results showed only a marginal effect for the absence of MAVS or TICAM-1 compared to WT mice. The results suggested that the pathways involving these two adaptor proteins were dispensable for triggering the immune responses that suppressed HBV replication.

To determine whether the RIG-I/MDA5-MAVS and TLR3-TICAM-1 RNA-sensing pathways were dispensable for suppressing the HBV replication, similar studies were performed in mice lacking both the MAVS and TICAM-1 adaptor proteins (fig. 1c). No notable differences were observed between WT and MAVS/TICAM-1 double-knockout mice in serum HBsAg and HBV-DNA levels, consistent with other data obtained. In addition, similar kinetics of intrahepatic clearance of the HBV template as well as HBV replication was observed in WT, *Mavs*$^{-/-}$, and *Ticam-1*$^{-/-}$ mice as revealed by Southern blotting using HBV-specific probes (online suppl. fig. 1).

To ensure the efficiency of delivery of the HBV transcriptional template into the mouse liver, a plasmid harboring the *lacZ* gene was used to transfect the liver cells using the hydrodynamic injection method. X-gal (a substrate for *lacZ*) staining showed that nearly the entire liver of injected mice has successfully received the injected plasmid (online suppl. fig. 2). An independent determination of transfection efficiency was carried out using a plasmid harboring the GFP fragment. The comparable transfection efficiencies observed did not differ significantly among the different mouse strains (data not shown). Furthermore, quantification of HBV mRNA in the organs of WT and knockout mice on day 3 after hydrodynamic injection revealed that HBV mRNA was amplified mainly in the liver but not in other organs, including kidney, lung, heart, spleen, and thymus (online suppl. fig. 3). Only weak HBV signals were detected in other organs in some types of knockout mice. These results demonstrated that HBV replication in vivo using the injection method was efficient and liver specific.

To further assess the possibility of HBV RNA acting as pathogen-associated molecular patterns to trigger the induction of type I IFN in hepatocytes, we transfected the immortalized hepatocytes with a plasmid containing the full genome of HBV as well as RNA containing the HBV mRNA. Along with the synthetic analog of dsRNA, poly(I:C), as a control, we determined the activity of the IFN-β promoter upon the stimulation using reporter gene assay (online suppl. fig. 4). Unlike poly(I:C), neither the full genome of HBV nor RNA induced any activity of the type I IFN promoter in the immortalized hepatocytes. Furthermore, we quantified the endogenous expression of genes including *cGas*, *Sting*, and *Mavs* in the hepatocyte cell lines in order to access the intrinsic RNA or DNA-sensing pathways (online suppl. fig. 5). We found that the hepatocyte cell lines, including those originating from mice and humans, expressed extremely low amounts of *Sting* compared to the intrinsic *Mavs*. However, other cell lines, including RAW 264.7 (murine macrophage cell line) and L929 (murine fibrosarcoma cell line), have higher endogenous expression of *Sting* in comparison to *Mavs*.

IRF-3/IRF-7 and IFNAR Are Critical Factors for HBV Replication Regulation

To investigate the mechanisms underlying the rapid termination of HBV replication in WT mice, we examined HBV clearance in IRF-3-/IRF-7-deficient mice. Activation of transcription factors including IRF-3 or IRF-7 is essential for raising immune responses including IFN production [25]. Unlike *Mavs*$^{-/-}$, *Ticam-1*$^{-/-}$, or WT mice, mice lacking the transcription factors IRF-3/IRF-7 had

Fig. 1. IFNAR and IRF-3/IRF-7 are critically associated with regulation of HBV propagation in mice but not MAVS and/or TICAM-1. HBsAg or HBV DNA were measured with sera from *Mavs*$^{-/-}$ (n = 13) (**a**), *Ticam-1*$^{-/-}$ (n = 10) (**b**), *Ticam-1*$^{-/-}$/*Mavs*$^{-/-}$ (n = 6) (**c**), *Irf-3*$^{-/-}$/*Irf-7*$^{-/-}$ (n = 12) (**d**), and *Ifnar*$^{-/-}$ (n = 13) (**e**) mice compared to WT mice (n = 15). These mice were hydrodynamically injected with 50 μg of the pTER-1.4xHBV plasmid containing full-genome HBV DNA. Mouse sera were isolated at the time points indicated. The HBsAg titers in the 1,000-fold diluted serum (left) and HBV DNA (right) in the knockout mice (●) were compared to the WT mice (○). Serum HBsAg titers were determined with an enzyme immunoassay at O.D. 450 nm [calculated as signal-over-noise ratios (S/N)]. Sera HBV DNA were determined by Q-PCR and indicated as copies per milliliter. Error bars indicate SD. The statistical p values were analyzed and no significant differences were observed in **a–c**. * $p < 0.01$ in **d** and **e** are time points statistically different between WT and transgenic mice.

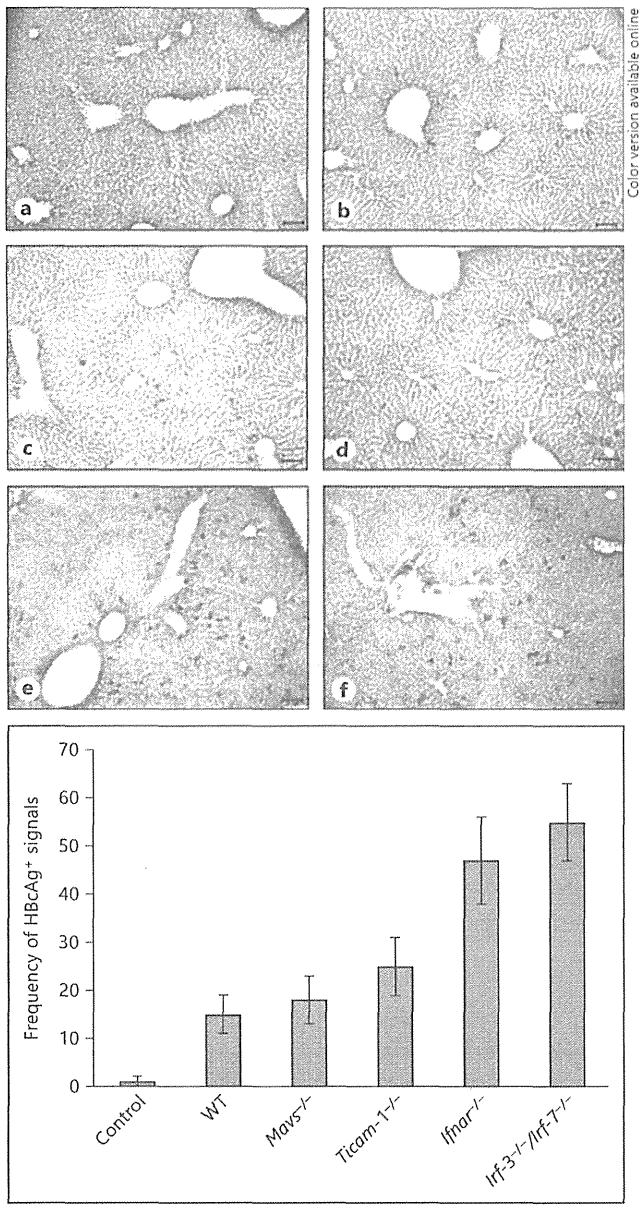

Fig. 2. Lacking IFNAR and IRF-3/IRF-7 causes an increase of HBcAg in mouse liver injected with the HBV replicative plasmid. The HBc protein in the livers on day 3 after injection was visualized with immunohistochemical staining of the mice liver sections embedded in OCT using an anti-HBc antibody for HBcAg. Representative sections are shown. HBcAg-positive cells were absent in the WT mice that received only the control plasmid (**a**). Only marginal differences were observed in the frequency of HBcAg-positive cells between WT (**b**), *Mavs*$^{-/-}$ (**c**), and *TICAM-1*$^{-/-}$ (**d**) mice. Frequency of HBcAg-positive cells in the livers of the *Ifnar*$^{-/-}$ (**e**) and *Irf-3*$^{-/-}$/*Irf-7*$^{-/-}$ (**f**) mice are more prevalent compared to the WT mice. The scale bars represent 10 μm. The images are displayed at 200× magnification. Frequency of HBcAg-positive signals between the different mouse strains shown is based on 3 images of each.

markedly high amounts of HBsAg and HBV DNA in sera (fig. 1d). A sharp peak of HBsAg in sera occurred in *Irf-3*$^{-/-}$/*Irf-7*$^{-/-}$ mice on day 4 after injection. However, in spite of the high virus titer at the early stage, HBsAg and DNA in sera were cleared with kinetics that paralleled the WT mice response, and viremia was eliminated by day 11. Hence, the substantial differences in the serum viremia between WT and *Irf-3*$^{-/-}$/*Irf-7*$^{-/-}$ mice in the early stage after transfection presumably reflects the importance of the genes being expressed with these transcription factors in the suppression of the HBV replication. IRF-3 and IRF-7 are the key molecules in the suppression of HBV viremia in the early stage after HBV injection.

Since type I IFN stimulates the IFNAR pathway to amplify type I IFN production, we hydrodynamically transfected HBV plasmid into mice lacking the gene of the type I IFN receptor (*Ifnar*$^{-/-}$) and assessed the suppression of HBV replication. *Ifnar*$^{-/-}$ mice showed markedly high titers of viral DNA and antigens in sera (fig. 1e) similar to *Irf-3*$^{-/-}$/*Irf-7*$^{-/-}$ mice.

The presence of HBcAg-positive hepatocytes was also monitored by immunohistochemical staining of liver sections from mice of each strain at day 4 after the injections (fig. 2). Data from the observed HBcAg-positive hepatocytes were in good agreement with the results on sera HBsAg and HBV DNA: only deficiency of IRF-3/IRF-7 and IFNAR resulted in a sharp increase of viremia in mice in the early stage (earlier than day 4). Fewer HBcAg-positive hepatocytes were observed in *Mavs*$^{-/-}$ and *Ticam1*$^{-/-}$ as well as WT mice at day 4 after injection than in *Irf-3*$^{-/-}$/*Irf-7*$^{-/-}$ or *Ifnar*$^{-/-}$ mice (fig. 2).

To gain insight into cytokine production in the liver in response to the HBV genome and its replication, we quantified the expression of type I IFN, IFN-γ, IL-7, IL-12p40, and chemokines including CXCL9, CXCL10, and CXCL11 mRNA in the livers of WT mice receiving either the control plasmid or plasmid carrying the HBV full genome on days 1, 3, 7, and 10 after hydrodynamic injection. Replication of HBV in the liver did not cause any significant changes in the expression of the cytokines or chemokines except the IFNs and CXCL-10 (fig. 3a–h). A similar study was carried out in WT and *Ifnar*$^{-/-}$ mice in order to further elaborate the type I IFN production. The IFNs increased in WT mice livers receiving the HBV full genome compared to the mouse livers receiving the control plasmid (fig. 3i–k). This increase was not observed in *Ifnar*$^{-/-}$ mice lacking the INF receptor. Although there appeared to be slight individual-to-individual differences in the apparent peaks of IFN-α induction, the result indicated that IFN-β was responsible for suppressing HBV